

# Our Response to Anonymous Referee #1

## General Comments

This manuscript addresses an important area of research, improving our ability to model and map hydrological interactions between wetlands and streams. It is well written and creative in its integration of methods, however the paper becomes a little confusing and muddled in interpreting whether theoretical or actual connectivity was modeled. In addition the inundation map does not appear to be validated. General and specific comments are below.

**RESPONSE:** We thank the reviewer for his/her thorough review and very helpful comments/suggestions. The positive feedback encourages us to continue working on this subject in the future.

1) The Introduction provides a strong background of the PPR, but could be strengthened by clarifying the novelty of the approach. Right now this is limited to stating that few studies of prairie wetlands have treated wetlands and catchments as integrated units and lidar is rarely used at broad scale but no citations are offered. Has this approach been used in other wetland landscapes, just not in the PPR? Or is this approach actually quite novel? What about related studies that have mapped wetland depressions and/or delineated wetland catchments? How does this approach fit in with those studies? Adding just a few sentences to discuss this would help contextualize the work presented.

**RESPONSE:** We thank the reviewer for the useful comments. We have revised this section and added appropriate references to justify the novelty of our approach.

“To our knowledge, little work has been done to delineate potential flow paths between wetlands and stream networks and use flow paths to characterize hydrologic connectivity in the PPR. In addition, previous remote sensing-based work on the hydrology of prairie wetlands mainly focused on mapping wetland inundation areas (e.g., Huang et al., 2014; Vanderhoof et al., 2017) or wetland depressions (e.g., McCauley and Anteau, 2014; Wu and Lane, 2016), few studies have treated wetlands and catchments as integrated hydrological units. Therefore, there is a call for treating prairie wetlands and catchments as highly integrated hydrological units because the existence of prairie wetlands depends on lateral inputs of runoff water from their catchments in addition to direct precipitation (Hayashi et al., 2016). Furthermore, hydrologic models for the PPR were commonly developed using coarse-resolution DEMs, such as the 30-m National Elevation Dataset (see Chu, 2015; Evenson et al., 2015; Evenson et al., 2016). High-resolution light detection and ranging (LiDAR) data have rarely been used in broad-scale (e.g., basin- or subbasin-scale) studies to delineate wetland catchments and model wetland connectivity in the PPR.”

2) Right now the last paragraph of the introduction is essentially a summary of what the paper did, but it would be stronger if the authors added what the goals, objectives, or research questions were. . .for example, our goal was to demonstrate a method to map potential hydrologic connections between wetlands and the river networks. . .

**RESPONSE:** Good suggestion. We have revised this paragraph and made our research objectives clear.

“In this paper, we present a semi-automated framework for delineating nested hierarchical wetland depressions and their corresponding catchments as well as simulating wetland connectivity using high-resolution LiDAR data. Our goal was to demonstrate a method to characterize fill-spill wetland hydrology and map potential hydrological connections between wetlands and stream networks. The hierarchical structure of wetland depressions and catchments was identified and quantified using a localized contour tree method (Wu et al., 2015). The potential hydrologic connectivity between wetlands and streams was characterized using the least-cost path algorithm. We also utilized high-resolution LiDAR intensity data to delineate wetland inundation areas, which were compared against the National Wetlands Inventory (NWI) to demonstrate the hydrological dynamics of prairie wetlands. Our ultimate goal is to build on our proposed framework to improve overland flow simulation and hydrologic connectivity analysis, which subsequently may improve the understanding of wetland hydrological dynamics at watershed scales.”

3) In calculating flow paths it is sometimes acknowledged that these are potential and sometimes stated that temporary and intermittent flowpaths have been identified. It should be made clear that these are potential hydrologic connections that are identified via the flowpaths, as it is not shown currently in the paper how or if active flowpaths are or could be distinguished from inactive flowpaths. However, the authors also mapped inundation and depressions, couldn't these be used to determine which depressions were connected? It isn't entirely clear if this is what is presented partially in Figure 10 or not.

**RESPONSE:** In the revised version, we have made it clear that the derived flow paths are potential hydrologic connections. We tried to distinguish active flow paths from inactive flow paths by visually assessing the derived flow paths overlaid on aerial photographs. Although we were not able to conduct quantitative assessments, we did find that the many potential flow paths were collocated with vegetated areas, which indicates that flow paths are likely located in high soil moisture areas that are directly or indirectly related to surface water or groundwater connectivity. The inundation areas were derived from the LiDAR intensity data, whereas the depressions were derived from the LiDAR DEM. Theoretically, the inundation areas are a subset of the depressions. In other words, the depressions represent the maximum ponded extents for the inundation areas. Since the LiDAR data were acquired during an extremely wet period, many wetlands already coalesced with adjacent wetlands to form larger wetland complexes. We could use dry-period aerial photographs to determine which depressions were connected. The LiDAR data can be used to show which depressions might potentially connect, but it cannot tell which depressions were actually connected.

4) It does not appear that the inundation map has been validated. Because of a lack of date match between the NAIP imagery and the LiDAR collection date, the NAIP imagery, appropriately, is primarily used to show that surface water changes over time. I realize it is challenging to validate maps classified from high resolution imagery but given the nearby Cottonwood site which monitors water levels at multiple ponds, are there field-measured water levels collected at a close date that could be used to help validate the inundation map?

**RESPONSE:** We thank the reviewer for this good suggestion. We have looked into the in-situ water-level data of the Cottonwood Lake Study Area retrieved from the USGS website (Mushet et al. 2016). We chose the field-measured water levels collected on October 27, 2011, which was the closest date to the LiDAR data acquisition date used in this study. The water levels of eight semi-permanent wetlands numbered through P1-P8 were used to compare the water elevation of wetland inundation areas derived using LiDAR data. The water level difference between the field measurement and LiDAR-derived measurement for these eight wetlands ranged from -5 cm to 11 cm, with an average

elevation difference of 0.5 cm, which falls within the vertical accuracy of the LiDAR DEM (15.0 cm). We have also made the inundation map available online at <http://wetlands.io/maps/inundation.html>.

Wetland ID	P01	P02	P03	P04	P06	P07	P08	Average
Field-measured (m)	560.30	561.01	557.86	561.01	562.55	562.76	556.66	NA
LiDAR-derived (m)	560.22	561.12	557.91	561.12	562.50	562.71	556.61	NA
Water-level difference (m)	-0.08	0.11	0.05	0.11	-0.05	-0.05	-0.05	0.0057

David M. Mushet, Donald O. Rosenberry, Ned H. Euliss, Jr., and Matthew J. Solensky, 2016, Cottonwood Lake Study Area - Water Surface Elevations. U.S. Geological Survey Data Release, <http://dx.doi.org/10.5066/F7707ZJ6>

5) I think the conclusion that dry NWI wetlands are likely no longer wetlands is a bit of a stretch. The PHDI does not consider snowmelt and is just based on rainfall and temperature, as the LiDAR collection was in October it is entirely possible that a large number of these wetlands are temporarily wet for few weeks in the spring following snowmelt. I don't think you can assume that these NWI wetlands no longer function as wetlands given just 1 fall date of inundation, even if in a wet year.

**RESPONSE:** We thank the reviewer for this concern. In the revised version, we have removed the statement that those 'dry' NWI wetlands are no longer wetlands. We have added more explanations about the discrepancy between NWI wetlands and our results derived by the LiDAR data.

"It is worth noting that most of these 'dried' NWI wetlands were relatively small with a median size of  $1.2 \times 10^3 \text{ m}^2$  (Table 2). The LiDAR intensity data were acquired in late October 2011, an extremely wet month according to the Palmer Hydrological Drought Index (Fig. 6). During this wet season, most wetlands would be expected to have abundant standing water. If no standing water could be detected in a wetland patch during this extremely wet period, it is possible that some of these small wetlands might have dried out during the past weeks to months. It is possible that land use change surrounding the 'dried' wetlands (e.g., row-cropping replacing pasture lands) may have affected their hydrology (Wright and Wimberly, 2013); water diversion via drainage or ditches could also be responsible for the lack of inundation, though we did not explore either of these potential drivers of change in this study. However, it is also likely that some of the 'dried' wetland might become wet again in the spring following snowmelt. The 'dried' NWI wetlands could also be attributed to the source of error in the original NWI data, which has a minimum mapping unit (i.e., the minimum sized wetland that can be consistently mapped) of 0.1 ha for the PPR (Tiner, 1997). Figure 5(b) shows that 37% of the 'dried' NWI polygons are smaller than the minimum mapping unit ( $1000 \text{ m}^2$ ). This implies that these small 'dried' NWI polygons could be due to the NWI mapping error."

## Minor Comments

Line 27 – grammatical error, change “highly” to “most” and modify sentence to avoid using “as” twice.

**RESPONSE:** We have revised the sentence as suggested.

Line 32 – awkward sentence, change to “the potholes range in size from”

**RESPONSE:** We have revised the sentence as suggested.

Line 34 – the term ephemeral is more commonly used for streams, the term “temporary” is more commonly used for wetlands.

**RESPONSE:** We have changed “ephemeral” to “temporary”

Line 37 – remove the word “as”

**RESPONSE:** We have removed “as”.

Line 39 – conterminous is misspelled

**RESPONSE:** We have corrected the typo.

Line 94 – change to “collected in late October”

**RESPONSE:** We have revised the sentence as suggested.

Line 97 – add space between in and 15.0 cm.

**RESPONSE:** Space added.

2.2. LiDAR Data – I realize you mention this in the Discussion, but it would be helpful to also add quick comment here regarding how wet October 2011 was and how this may have influenced the resulting DEM.

**RESPONSE:** We thank the author for the good suggestion. We have added the following sentences to the end of this section: “It is worth noting that October 2011 was an extreme wet period according to the Palmer Hydrological Drought Index. Consequently, small individual wetland depressions nested within larger inundated wetland complexes might not be detectable from the resulting LiDAR DEM.”

Line 126 – change “these” to “the”

**RESPONSE:** We have changed “these” to “the”.

Comment - In the Methodology section change from present tense to past tense.

**RESPONSE:** We have revised the Methodology section as suggested. For specific data processing steps we performed, we used the past tense. When describing diagrams not tied to specific data processing steps we performed, we used the present tense.

Line 215 – add the word “of” between number and upslope.

**RESPONSE:** We have added the word “of”.

Section 3.2 – I’m assuming to use the contour approach you need to convert the DEM to vectors. . .is any information lost in this process? why not just use a raster-based approach to find depressions?

**RESPONSE:** To the best of our knowledge, there is no raster-based approach available to delineate and characterize the nested hierarchical structure of depressions. The traditional sink-filling method can delineate the maximum extent of a composite depression. However, it cannot distinguish or delineate the individual depressions (if any) nested within the composite depression. Moreover, the topological relationship between nested depressions cannot be derived from the raster-based approach. The vector-based contour-tree approach used in this study can not only identify nested depressions but also characterize their topological relationships, which are crucial for studying the filling-merging-spilling hydrology. In this study, we set the contour interval as 20 cm, which was chosen based on the LiDAR vertical accuracy (15 cm) and consideration of computational time. Like any other vector-raster data conversion process, there might be some information lost in this process. Nevertheless, we believe that the contour interval of 20 cm is sufficient to minimize the information loss based on our experiments. An in-depth discussion about the contour interval selection is available in the Wu et al. (2015) paper.

Section 3.4 – In calculating ponding time, are you assuming no infiltration? If so, add this as an assumption to the text.

**RESPONSE:** We have added the following sentences to this section: “For the sake of simplicity, we made two assumptions. First, we assumed that the rainfall was temporally and spatially consistent and uniformly distributed throughout the landscape and all surfaces were impervious. Second, we assumed no soil infiltration.”

Section 3.4 – Does the water storage capacity, and in turn the ponding time equations assume the depression is dry to start with? How is the pre-existing water in the depressions dealt with? This is particularly an issue for permanent wetlands.

**RESPONSE:** We did not assume the depression is dry to start with. The ponding time of a depression was calculated based on the potential water storage and its corresponding catchment area. In other words, we don’t need the existing water storage to calculate the ponding time. It does not matter whether a depression is dry or has existing water. If a depression is completely dry without any existing water, the potential water storage refers to the storage volume between the lowest point and the spilling point of the depression. If a depression has existing water in it, the potential water storage refers to the potential water volume the depression can hold between the water surface and the spilling point. The potential water storage capacity of each wetland depression was computed through statistical analysis of the LiDAR DEM grid cells that fall within the depression. The calculation of existing water storage is not the focus of this study. Since the near-infrared LiDAR sensors generally could not penetrate water, the depression morphology beneath the water surface could not be derived from LiDAR data. Therefore, it is not possible to calculate the exact storage volume of an existing waterbody. However, many studies have showed that there is a strong statistical relationship between

storage volume and surface area in a depression (e.g., see Gleason, et al. (2007), Wu and Lane (2016)). Therefore, existing water storage can be estimated using empirical equations if needed.

- 1) Gleason, R. A., B. A. Tangen, M. K. Laubhan, K. E. Kermes and N. H. Euliss Jr. 2007. Estimating water storage capacity of existing and potentially restorable wetland depressions in a subbasin of the Red River of the North. p. 36. U.S. Geological Survey Open-File Report 2007-1159.
- 2) Wu, Q. and C. R. Lane. 2016. Delineation and Quantification of Wetland Depressions in the Prairie Pothole Region of North Dakota. *Wetlands*, 36:215-227.

Comment – what was the range of rainfall intensities that were added to derive the ponding time estimates?

**RESPONSE:** For this study, we used a uniform steady rainfall with an intensity of 5.0 cm/h based on the literature (e.g., see Chu (2015)). The rainfall intensity can be easily adapted in other study areas to derive the ponding time estimates.

- 1) Chu, X. 2015. Delineation of Pothole-Dominated Wetlands and Modeling of Their Threshold Behaviors. *Journal of Hydrologic Engineering*: D5015003.

Line 287-310 This paragraph is methods and should be moved to the Methods section accordingly.

**RESPONSE:** We have moved this paragraph to the Methodology section as suggested.

Line 303-304 – What about inundation in streams that may not have been mapped as depressions, would these inundation objects be lost given this filtering step?

**RESPONSE:** Based on our visual assessments, no major inundation areas along streams were missed during the filtering step. In other others, all major inundation areas along streams were mapped as depressions. The inundation mapping results overlaid on the LiDAR intensity imagery are available for viewing at <http://wetlands.io/maps/inundation.html>.

Section 4.2 How common was it for wetland depressions to be nested within a larger catchments? Is there a way this nested hierarchy could be quantified or showed?

**RESPONSE:** The fill-and-spill hydrology in the Prairie Pothole Region is well documented in the literature. It is very common for wetland depression to be nested within a larger catchment. In our study, the nested hierarchy was quantified and characterized using the localized contour tree approach. A conceptual diagram of the approach is shown in Figure 4. Real-world examples demonstrating the fill-spill process and nested hierarchy can be seen from the time-series aerial images shown in Figure 2.

Line 362-363 – Although the findings are based on a much larger sample size, they are also all derived from a single watershed, so the results may also be site specific.

**RESPONSE:** It is true that our results are also site-specific. We have modified the sentence and stated that the results are “for the study area” only. Nevertheless, we believe that our results regarding the proportion of depression area to catchment area are statistically more reliable than that

reported in previous studies, which were calculated based on a very limited number (<20) of depressions. In contrast, our results were computed from more than 30,000 wetland depressions and catchments.

Section 4.3 – The flow paths are potential flow paths, however, right? Water may not have flowed along a fraction of them to date. This should be made clear in the text.

**RESPONSE:** We thank the reviewer for pointing this out. We have modified the text accordingly and made it clear that the flow paths derived in this study are potential flow paths.

Line 384 – remove “the” before late October

**RESPONSE:** We have removed “the”.

Line 385 – add “a” after such.

**RESPONSE:** We have added “a” after such.

Line 388-389 - revise sentence to “A substantial number of inundated NWI wetlands were found to coalesce with adjacent wetlands. . .”

**RESPONSE:** We have revised the sentence as suggested.

Line 402 – Do you mean you “could” use it if a dry-period LiDAR was available?

**RESPONSE:** Yes, this is what we meant. We have changed “can” to “could”.

Line 384-406 – This is a good discussion of an important issue but it is not entirely clear how this issue affected your findings in this case. I would guess that you likely under-estimated the number of depressions that coalesced?

**RESPONSE:** We thank the reviewer for the encouraging comment. We have to admit that our findings were inevitably affected by the LiDAR data used in this study. Since the LiDAR data were acquired during an extreme wet period, many wetlands already coalesced with adjacent wetlands to form larger wetland complexes. Therefore, it is not possible delineate the individual wetlands before they coalesced unless we had another LiDAR dataset acquired during a dry period. Our methods focused on the potential coalescence between adjacent wetlands when water levels in wetlands continued to increase rather than the coalescence that already took place. In an ideal situation, i.e., the LiDAR data is acquired during an extremely dry period, our methods can simulate the filling-merging-spilling processes and project the coalescences between wetlands. The results can then be validated using the wet-period LiDAR data and aerial photographs.

Line 404-405 – As far as I can tell, however, in this case you did not use the time-series or wet inundation to evaluate or summarize fill-and-spill patterns. Is this correct?

**RESPONSE:** It is correct that we were not able to use the wet-period LiDAR data to evaluate the fill-and-spill patterns. This is partly due to the limitation of the LiDAR data. As noted in the paper, the LiDAR data used in this study were acquired in late October 2011, which was an extremely wet period according to the Palmer Hydrological Drought Index. During such a wet period, a substantial number of inundated wetlands were found to coalesce with adjacent wetlands and form larger wetland complexes. As a result, we were not able to obtain the information of basin morphology of individual depressions before they merged into large wetland complexes. Ideally, using multiple LiDAR datasets acquired in both dry and deluge conditions in conjunction with time-series aerial photographs would be essential for studying the fill-and-spill mechanism of prairie wetlands. In this case, we could use the dry-period LiDAR data to delineate and characterize the morphology of individual wetland depressions before the fill-and-spill processes occur. Furthermore, we can derive the potential flow paths and project the coalescing of wetland depressions after the fill-and-spill processes initiate. The wet-period LiDAR data and time-series aerial photographs can serve as validation datasets to evaluate the fill-and-spill patterns. We plan to further investigate this issue when a dry-period LiDAR data for our study area becomes available.

Line 425 – Can't use the word "accurately" if no validation was done.

**RESPONSE:** We have removed the word "accurately".

Line 433 – Add "potential" before hydrological connectivity.

**RESPONSE:** We have added the word "potential" before hydrological connectivity.

Line 435 – I am struggling with this statement which is used several times throughout the manuscript. Although temporary or seasonal flow paths were likely identified, flowpaths were also likely identified that never actually carry water. How can we distinguish between these or can we?

**RESPONSE:** We thank the reviewer for this concern. We have made changes throughout the manuscript and made it clear that all flow paths identified in this study are potential flow paths. By examining the potential flow paths overlaid on the color infrared aerial photograph, we found that many potential flow paths appeared to be collocated with vegetated areas (see Fig. 9(b)). This indicates that flow paths are likely located in high soil moisture areas that are directly or indirectly related to surface water or groundwater connectivity. We agree with the reviewer that some potential flow paths might never actually carry water. We plan to further investigate this issue in a follow-up study to categorize and validate potential flow paths.

Line 439 –Add what the specific limiting factors have been with traditional remote sensing methods.

**RESPONSE:** We have modified the sentence as suggested: "Broad-scale prairie wetland hydrology has been difficult to study with traditional remote sensing methods using multi-spectral satellite data due to the limited spatial resolution and the interference of tree canopy (Klemas, 2011; Gallant, 2015)."



- 1) Klemas, V.: Remote sensing of wetlands: case studies comparing practical techniques, *Journal of Coastal Research*, 27, 418-427, 2011.
- 2) Gallant, A.: The Challenges of Remote Monitoring of Wetlands, *Remote Sensing*, 7, 10938, 2015.

Table 1 – remove extra spaces between Freshwater and Emergent.

**RESPONSE:** We have removed the extra spaces.

Figure 5, 8 and 10 – I would add a basic color to the histograms, maybe light gray? To improve the aesthetics.

**RESPONSE:** We have modified all histograms as suggested.

Figure 6 – Modify x-axis to just show year

**RESPONSE:** We have modified the x-axis as suggested.

Figure 7 – the yellow and blue lines are hard to see, maybe making them a little thicker might make them more visible.

**RESPONSE:** We have made the lines thicker. In addition, we switched the line colors to make them consistent with those shown in Figure 9. Yellow line and blue line represent NWI wetlands and LiDAR-derived inundation areas, respectively.

Figure 10 – This figure gets at several questions I had. Was connectivity calculated so that all wetlands connected to each other and eventually to a stream? And this is then the length distribution of those flowpath lines? If so it should be indicated that these are potential connectivity. What does connected wetlands mean here? Are these just the coalesced wetlands?

**RESPONSE:** We have modified the figure and corresponding text to indicate the potential wetland connectivity. Figure 10a shows the distribution of potential flow path lengths. Figure 10b shows the distribution of elevation differences between wetlands connected through the potential flow paths.

## Our Response to Anonymous Referee #2

### General Comments

This manuscript was well thought out, well organized and well written. In the United States the regulatory status of wetlands is currently linked to connectivity to streams so the topic of this manuscript is important. The conceptual model presented for wetland fill and spill seems very useful. The approach used in the reported study is sound and findings support the conclusions reached.

**RESPONSE:** We thank the reviewer for the encouraging comments.

### Specific comments:

The last paragraph of the introduction is a summary of the study findings. It should be modified to reflect study goals instead.

**RESPONSE:** We thank the reviewer for the good suggestion. We have revised this paragraph and made our research objectives more clear.

“In this paper, we present a semi-automated framework for delineating nested hierarchical wetland depressions and their corresponding catchments as well as simulating wetland connectivity using high-resolution LiDAR data. Our goal was to demonstrate a method to characterize fill-spill wetland hydrology and map potential hydrological connections between wetlands and stream networks. The hierarchical structure of wetland depressions and catchments was identified and quantified using a localized contour tree method (Wu et al., 2015). The potential hydrologic connectivity between wetlands and streams was characterized using the least-cost path algorithm. We also utilized high-resolution LiDAR intensity data to delineate wetland inundation areas, which were compared against the National Wetlands Inventory (NWI) to demonstrate the hydrological dynamics of prairie wetlands. Our ultimate goal is to build on our proposed framework to improve overland flow simulation and hydrologic connectivity analysis, which subsequently may improve the understanding of wetland hydrological dynamics at watershed scales.”

Flow routing was performed using D8 algorithm (line 213) but often it has been found that D-infinity algorithms provide more realistic flow characteristics.

**RESPONSE:** We agree with the reviewer that D-infinity algorithms might provide more realistic flow characteristics. In our study, the flow direction raster was generated and used as an intermediate dataset to derive wetland catchments. For delineating catchments/watersheds, we tried the ArcGIS Hydrology Toolbox (<https://goo.gl/GhmFId>) and the open-source Whitebox Geospatial Analysis Tools (<https://goo.gl/dqV4cE>). Both software packages use D8 algorithm for watershed delineation. Since our data processing flow was built on the ArcGIS Hydrology Toolbox, for the sake of simplicity, we used the D8 algorithm available in ArcGIS to derive flow directions. Nevertheless, we believe that both flow direction algorithms should lead to the same watershed delineation results.

When reporting numerical results consider the errors associated with the underlying model used to produce the values. The number of nonzero digits should generally reflect the uncertainty. For example see lines 347 and 348 with values reported with 4 significant figures whereas it is known that

these estimates have substantial uncertainty. Also in tables with data reported with up to 8 significant digits (Tables 1 to 4).

**RESPONSE:** We appreciate this concern. In the revised manuscript, we have reduced the number of significant digits to no more than three throughout the manuscript.

Figure 7 needs to be reworked. Labels on figure are very difficult to read

**RESPONSE:** We have revised Figure 7. We made the lines thicker. In addition, we switched the line colors to make them consistent with those shown in Figure 9. Yellow line and blue line represent NWI wetlands and LiDAR-derived inundation areas, respectively.

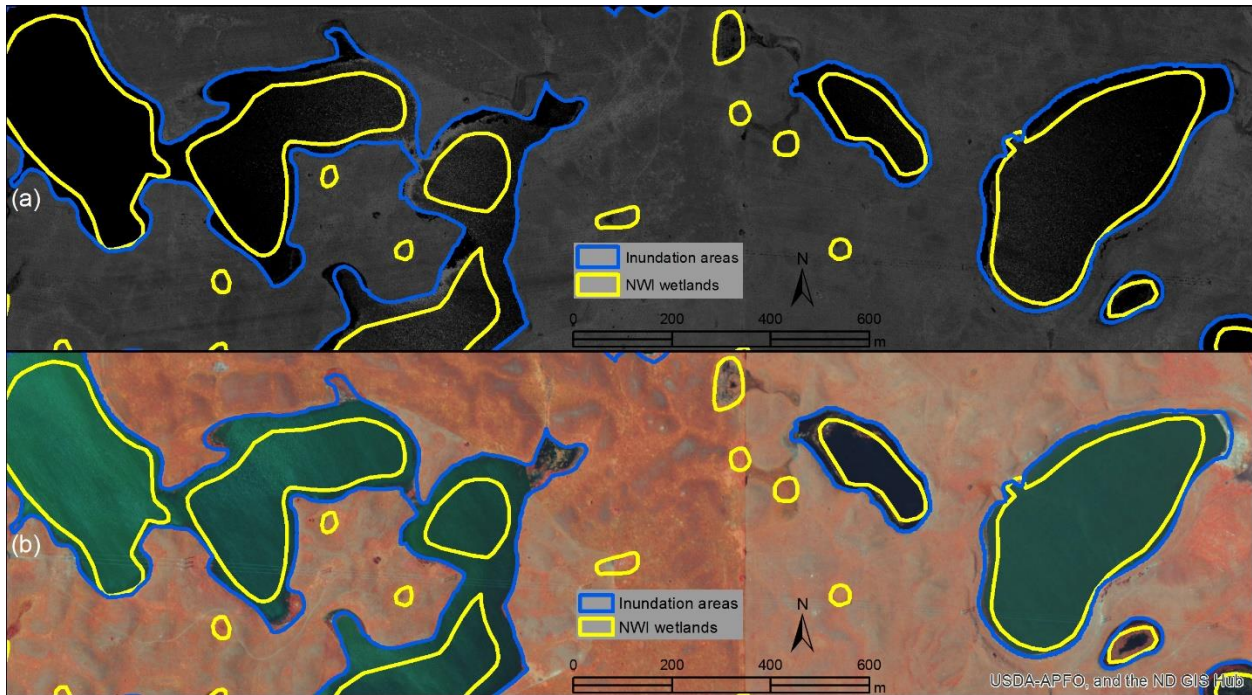


**Figure 7.** Comparison between inundation areas (derived from LiDAR intensity data) and NWI wetland polygons

# Delineating wetland catchments and modeling hydrologic connectivity using LiDAR data and aerial imagery

Qiusheng Wu<sup>1</sup>, Charles R. Lane<sup>2</sup>

<sup>1</sup>Department of Geography, Binghamton University, State University of New York, Binghamton, NY 13902, USA

<sup>2</sup>U.S. Environmental Protection Agency, Office of Research and Development, National Exposure Research Laboratory, 26 W. Martin Luther King Dr., Cincinnati, OH 45268, USA

Correspondence to: Qiusheng Wu ([wqs@binghamton.edu](mailto:wqs@binghamton.edu))

**Abstract:** In traditional watershed delineation and topographic modeling, surface depressions are generally treated as spurious features and simply removed from a digital elevation model (DEM) to enforce flow continuity of water across the topographic surface to the watershed outlets. In reality, however, many depressions in the DEM are actual wetland landscape features with seasonal to permanent inundation patterning characterized by nested hierarchical structures and dynamic filling-spilling-merging surface-water hydrological processes ~~that are seldom fully filled with water.~~ Differentiating and appropriately processing such ecohydrologically meaningful features remains a major technical terrain-processing challenge, particularly as high-resolution spatial data are increasingly used to support modeling and geographic analysis needs. ~~For instance, wetland depressions in the Prairie Pothole Region (PPR) are seasonally to permanently flooded wetlands characterized by nested hierarchical structures with dynamic filling-spilling-merging surface-water hydrological processes.~~ The objectives of this study were to delineate hierarchical wetland catchments and model their hydrologic connectivity using high-resolution LiDAR data and aerial imagery. The graph theory-based contour tree method was used to delineate the hierarchical wetland catchments and characterize their geometric and topological properties. Potential hydrologic connectivity between wetlands and streams were simulated using the least-cost path algorithm. The resulting flow network delineated putative temporary or seasonal potential flow paths connecting wetland depressions to each other or to the river network at scales finer than available through the National Hydrography Dataset. The results demonstrated that our proposed framework is promising for improving overland flow simulation and hydrologic connectivity analysis.

**Keywords:** flow path, geographically isolated wetlands, hydrologic connectivity, LiDAR, prairie pothole, wetland depressions, ~~geographically isolated wetlands, flow path, LiDAR~~

## 1 Introduction

The Prairie Pothole Region (PPR) of North America extends from the north-central United States (U.S.) to south-central Canada, encompassing a vast area of approximately 720,000 km<sup>2</sup>. The landscape of the PPR is dotted with millions of wetland depressions formed by the glacial retreat that happened during the Pleistocene Epoch (Winter, 1989). The PPR is considered as one of the largest and highly-most productive wetland areas in the world, which as ~~it~~ serves as a primary breeding habitat for much of North America's waterfowl population (Keddy, 2010; Steen et

33 al., 2014; Rover and Mushet, 2015). The wetland depressions, commonly known as potholes, possess important  
34 hydrological and ecological functions, such as providing critical habitat for many migrating and breeding waterbirds  
35 (Minke, 2009), acting as nutrient sinks (Oslund et al., 2010), and storing surface water that can attenuate peak runoff  
36 during a flood event (Huang et al., 2011b). The potholes ~~size-ranges in size~~ from a relatively small area of less than  
37 100 m<sup>2</sup> to as large as 30,000 m<sup>2</sup>, with an estimated median size of 1600 m<sup>2</sup> (Zhang et al., 2009; Huang et al., 2011a).  
38 Most potholes have a water depth of less than 1 m with varying water permanency, ranging from ~~ephemeral~~  
39 ~~temporary~~ to permanent (Sloan, 1972). Due to their small size and shallow depth, these wetlands are highly sensitive  
40 to climate variability and are vulnerable to ecological, hydrological, and anthropogenic changes. Wetland  
41 depressions have been extensively drained and filled due to agricultural expansion, which is considered ~~as~~ the  
42 greatest source of wetland loss in the PPR (Johnston, 2013). In a report to the ~~United States (U.S.)~~ Congress on the  
43 status of wetland resources, Dahl (1990) estimated that the ~~con~~terminous U.S. lost more than 50 percent of ~~their-its~~  
44 original wetland ~~acreages~~ over a period of 200 years between the 1780s and the 1980s. More recently, Dahl (2014)  
45 reported that the total wetland area in the PPR declined by approximately 300 km<sup>2</sup> between 1997 and 2009. This  
46 represents an average annual net loss of 25 km<sup>2</sup>. Regarding the number of depressions, it was estimated that the  
47 wetland depressions declined by over 107,000 or four percent between 1997 and 2009 (Dahl, 2014).

48 The extensive wetland drainage and removal have increased precipitation runoff into regional river basins,  
49 which is partially responsible for the increasing frequency and intensity of flooding events in the PPR (Miller and  
50 Nudds, 1996; Bengtson and Padmanabhan, 1999; Todhunter and Rundquist, 2004). Concerns over flooding along  
51 rivers in the PPR have stimulated the development of hydrologic models to simulate the effects of depression  
52 storage on peak river flows (Hubbard and Linder, 1986; Gleason et al., 2007; Gleason et al., 2008; Huang et al.,  
53 2011b). Since most of these prairie wetlands do not have surface outlets or well-defined surface water connections,  
54 they are generally considered as geographically isolated wetlands (GIWs) ~~or upland-embedded wetlands~~ (Tiner,  
55 2003; Mushet et al., 2015; Cohen et al., 2016; Lane and D'Amico, 2016). Recently, the U.S. Environmental  
56 Protection Agency conducted a comprehensive review of over 1350 peer-reviewed papers with the aim to synthesize  
57 existing scientific understanding of how wetlands and streams affect the physical, chemical, and biological integrity  
58 of downstream waters (U.S. EPA, 2015). The report concludes that additional research focused on the frequency,  
59 magnitude, timing, duration, and rate of fluxes from GIWs to downstream waters is needed to better identify  
60 wetlands with ~~hydrological connections or~~ functions that ~~significantly-substantially~~ affect other waters and maintain  
61 the long-term sustainability and resiliency of valued water resources.

62 In addition to the comprehensive review by the U.S. EPA (2015), a number of recent studies focusing on the  
63 hydrologic connectivity of prairie wetlands have been reported in the literature. For example, Chu (2015) proposed a  
64 ~~puddle-to-puddle~~-modeling framework to delineate prairie wetlands and characterize their dynamic hydro-  
65 topographic properties in ~~a small North Dakota research area the Cottonwood Lake area~~ (2.55 km<sup>2</sup>) using a 10-m  
66 resolution digital elevation model (DEM). Vanderhoof et al. (2016) examined the effects of wetland expansion and  
67 contraction on surface water connectivity in the PPR using time series Landsat imagery. Ameli and Creed (2017)  
68 developed a physically-based hydrologic model to characterize surface and groundwater hydrologic connectivity of  
69 prairie wetlands. [These reported studies represent some of the latest research developments on hydrologic](#)

connectivity in the PPR. To our knowledge, little work has been done to delineate potential flow paths between wetlands and stream networks and use flow paths to characterize hydrologic connectivity in the PPR. In addition, previous remote sensing-based work on the hydrology of prairie wetlands mainly focused on mapping wetland inundation areas (e.g., Huang et al., 2014; Vanderhoof et al., 2017) or wetland depressions (e.g., McCauley and Anteau, 2014; Wu and Lane, 2016). few studies have treated wetlands and catchments as integrated hydrological units. Therefore, there is a call for treating ~~In a comprehensive overview of wetland hydrology in the PPR, Hayashi et al. (2016) highlighted that~~ prairie wetlands and catchments ~~should be considered~~ as highly integrated hydrological units because the existence of prairie wetlands depends on lateral inputs of runoff water from their catchments in addition to direct precipitation (Hayashi et al., 2016). ~~To our knowledge, however, few studies on the hydrology of prairie wetlands have treated wetlands and catchments as integrated hydrological units (McCauley and Anteau, 2014; Wu and Lane, 2016).~~ Furthermore, hydrologic models for the PPR were commonly developed using ~~course~~ coarse-resolution DEMs, such as the 30-m National Elevation Dataset ~~high-resolution light detection and ranging (LiDAR) data have rarely been used in broad scale (e.g., basin- or subbasin scale) studies to delineate wetland catchments and model wetland connectivity in the PPR (see Chu, 2015; Evenson et al., 2015; Evenson et al., 2016).~~ High-resolution light detection and ranging (LiDAR) data have rarely been used in broad-scale (e.g., basin- or subbasin-scale) studies to delineate wetland catchments and model wetland connectivity in the PPR.

In this paper, we present a semi-automated framework for delineating nested hierarchical wetland depressions and their corresponding catchments as well as simulating wetland connectivity using high-resolution LiDAR data. Our goal was to demonstrate a method to characterize fill-spill wetland hydrology and map potential hydrological connections between wetlands and stream networks. The hierarchical structure of wetland depressions and catchments was identified and quantified using ~~the-a~~ localized contour tree method (Wu et al., 2015). The potential hydrologic connectivity between wetlands and streams was characterized using the least-cost path algorithm. We also utilized high-resolution LiDAR intensity data to delineate wetland inundation areas, which were compared against the National Wetlands Inventory (NWI) to demonstrate the hydrological dynamics of prairie wetlands. ~~The resulting flow network delineated putative temporary or seasonal flow paths connecting wetland depressions to each other or to the river network at scales finer than available through the National Hydrography Dataset. The results demonstrated that our proposed framework is promising for improving~~ Our ultimate goal is to build on our proposed framework to improve overland flow simulation and hydrologic connectivity analysis, which subsequently may improve the understanding of wetland hydrological dynamics at watershed scales.

## 2 Study area and datasets

### 2.1 Study area

~~Our study~~ The work ~~area~~ focused on the Pipestem River subbasin in the Prairie Pothole Region of North Dakota (Fig. 1). The subbasin is an 8-digit Hydrologic Unit Code (#10160002) with a total area of approximately 2,770 km<sup>2</sup>, covering four counties in North Dakota (see Fig. 1). The climate of the subbasin is characterized by long, cold, dry winters and short, mild, variably wet summers (Winter and Rosenberry, 1995). Average annual precipitation is

105 approximately 440 mm with substantial seasonal and annual variations (Huang et al., 2011a). The land cover of the  
106 Pipestem subbasin is dominated by cultivated crops (44.1%), herbaceous vegetation (25.9%), and ~~payhay~~/pasture  
107 (13.1%), with a substantial amount of open water (7.1%) and emergent herbaceous wetlands (5.6%) (Jin et al.,  
108 2013). The Cottonwood Lake area (see the blue rectangle in Fig. 1), a long-term field research site established by the  
109 U.S. Geological Survey (USGS) and the U.S. Fish and Wildlife Service (USFWS) in 1977 for wetland ecosystem  
110 monitoring, has been a very active area of research for several decades (e.g., Sloan, 1972; Winter and Rosenberry,  
111 1995; Huang et al., 2011a; Mushet and Euliss, 2012; Hayashi et al., 2016).

## 112 2.2 LiDAR data

113 The LiDAR elevation data for the Pipestem subbasin were collected in ~~the~~ late October ~~of~~ 2011 and distributed  
114 through the North Dakota GIS Hub Data Portal (<https://gis.nd.gov/>, accessed December 30, 2016). The bare-earth  
115 digital elevation models (DEMs) derived from LiDAR point clouds are freely available as 1-m resolution image tiles  
116 (2 km × 2 km). The vertical accuracy of the LiDAR DEM is 15.0 cm. ~~In total, the Pipestem Subbasin consists of 786~~  
117 ~~DEM tiles with an aggregated file size of 22.66 GB.~~ We created a seamless LiDAR DEM (see Fig. 1) for the  
118 Pipestem subbasin by mosaicking 786 DEM tiles and used it for all subsequent data analyses (approximately 22.66  
119 GB file size). The elevation of the subbasin ranges from 422 m to 666 m, with relatively high-elevation areas in the  
120 west and low-elevation areas in the east.

121 The LiDAR intensity data for the Pipestem subbasin were also collected at 1-m resolution coincident with  
122 the LiDAR elevation data collection. In general, the return signal intensities of water areas are relatively weak due to  
123 water absorption of the near-infrared spectrum (Lang and McCarty, 2009; McCauley and Anteau, 2014). As a result,  
124 waterbodies typically appear as dark features whereas non-water areas appear as relatively bright features in the  
125 LiDAR intensity image. Thresholding techniques have been commonly used to distinguish water pixels from non-  
126 water pixels (Huang et al., 2011b; Huang et al., 2014; Wu and Lane, 2016). In this study, the LiDAR intensity data  
127 were primarily used to extract standing-water areas (i.e., inundation areas) while the LiDAR DEMs were used to  
128 derive nested wetland depressions and their corresponding catchments above the standing-water surface. It is worth  
129 noting that October 2011 was an extreme wet period according to the Palmer Hydrological Drought Index (Huang et  
130 al., 2011a). Consequently, small individual wetland depressions nested within larger inundated wetland complexes  
131 might not be detectable from the resulting LiDAR DEM.

## 132 2.3 Ancillary data

133 In addition to the LiDAR datasets, we used three ancillary datasets, including the 1-m resolution aerial imagery from  
134 the National Agriculture Imagery Program (NAIP) of the U.S. Department of Agriculture (USDA), the National  
135 Wetlands Inventory (NWI) from the USFWS, and the National Hydrography Dataset (NHD) from the USGS.

136 The NAIP imagery products were also acquired from the North Dakota GIS Hub Data Portal. The default  
137 spectral resolution of the NAIP imagery in North Dakota is natural color (Red, Green, and Blue, or RGB).  
138 Beginning in 2007, however, the state ~~data has have~~ been delivered with four bands of data: RGB and Near Infrared.  
139 We downloaded and processed six years of NAIP imagery for the Pipestem subbasin, including 2003, 2004, 2006,

140 2009, 2012, and 2014. A small portion of the study area with the NAIP imagery is shown in Fig. 2. These time-  
141 series NAIP imagery clearly demonstrate the dynamic nature of prairie pothole wetlands under various dry and wet  
142 conditions. In particular, the extremely wet year of 2014 resulted in many individual wetlands to coalesce and form  
143 larger wetland complexes (see the yellow arrows in Fig. 2). It should be noted that all the NAIP imagery were  
144 collected during the summer growing season of agricultural crops. Since no coincident aerial photographs were  
145 collected during the LiDAR data acquisition campaign in 2011, these NAIP imagery can serve as valuable data  
146 sources for validating the LiDAR-derived wetlands catchments and hydrological pathways in this study.

147 The NWI data for our study area were downloaded from <https://www.fws.gov/wetlands/> (accessed  
148 December 30, 2016). ~~These~~The wetlands inventory data in this region were created by manually interpreting aerial  
149 photographs acquired in the 1980s with additional support from soil surveys and field checking (Cowardin et al.,  
150 1979; Huang et al., 2011b; Wu and Lane, 2016). Tiner (1997) reported that the target mapping unit, the size class of  
151 the smallest group of NWI wetlands that can be consistently mapped, was between 1000 m<sup>2</sup> and 4000 m<sup>2</sup> in the  
152 Prairie Pothole Region. It should be noted that the target mapping unit is not the minimum wetland size of the NWI.  
153 In fact, there are a considerable amount of NWI wetland polygons smaller than the target mapping unit (1000 m<sup>2</sup>). In  
154 this study, we focused on the prairie wetlands that are greater than 500 m<sup>2</sup>. Therefore, 5644 small NWI wetland  
155 polygons (< 500 m<sup>2</sup>) were eliminated from further analysis. In total, there were 32,016 NWI wetland polygons (≥  
156 500 m<sup>2</sup>) across the Pipestem subbasin (Table 1). The total size of these NWI wetlands was approximately 279.5 km<sup>2</sup>,  
157 covering 10.1% of the Pipestem subbasin. The areal composition of NWI wetlands were freshwater emergent  
158 wetlands (86.5%), lakes (7.5%), freshwater ponds (5.3%), freshwater forested/shrub wetland (0.4%), and riverine  
159 systems (0.3%). The median size of wetlands (≥ 500 m<sup>2</sup>) in our study area was ~~4778~~ $1.8 \times 10^3$  m<sup>2</sup>. Although the  
160 NWI data is the only spatially comprehensive wetland inventory for our study area, it is now considerably out-of-  
161 date, as it was developed 30 years ago and it does not reflect the wetland temporal change (Johnston, 2013). The  
162 wetland extent and type for many wetland patches have changed since its original delineation (e.g., Fig. 2).  
163 Nevertheless, NWI does provide valuable information about wetland locations (Tiner, 1997; Huang et al., 2011b).  
164 Furthermore, the NWI definition of wetlands requires only one of three wetland indicators (soils, hydrology, or  
165 plants) whereas regulatory delineation requires all three [33 Code of Federal Regulations 328.3(b)]. In our study, the  
166 NWI polygons were primarily used to compare with the wetland depressions delineated from the LiDAR DEM.

167 The high-resolution NHD data were downloaded from <http://nhd.usgs.gov> (accessed December 30, 2016).  
168 There were 1840 polyline features in the NHD flowline layer for the Pipestem subbasin, with a total length of  
169 ~~1402.2~~ $1.4 \times 10^3$  km and an average length of 762 ~~4~~m. The NHD flowlines overlaid on top of the LiDAR DEM  
170 ~~with isare~~ shown in Fig. 1. It is worth noting that the majority of the NHD flowline features were found in the low-  
171 elevation areas in the east. The high-elevation areas in the west where most NWI wetland polygons are located have  
172 very few NHD flowlines, except for the Little Pipestem Creek. This ~~implies~~suggests that a large number of  
173 temporary and seasonal flow paths were not captured in the NHD dataset, perhaps due to the fact that, -It is also  
174 worth noting that the NHD does not try to systematically measure stream lines <1.6 km (Stanislawski, 2009; Lane  
175 and D'Amico, 2016). In this study, the NHD flowlines were used to compare the LiDAR-derived potential flow  
176 paths using our proposed methodology.



## 177 3 Methodology

### 178 3.1 Outline

179 Our methodology for delineating nested wetland catchments and flow paths is a semi-automated approach consisting  
180 of several key steps: (a) extraction of hierarchical wetland depressions using the localized contour tree method (Wu  
181 et al., 2015); (b) delineation of nested wetland catchments; (c) calculation of potential water storage; and (d)  
182 derivation of potential flow paths using the least-cost path search algorithm. The LiDAR DEM ~~is-was~~ used to  
183 delineate hierarchical wetland depressions and nested wetland catchments. The LiDAR intensity imagery ~~is-was~~  
184 used to extract wetland inundation areas. The potential water storage of each individual wetland depression ~~is-was~~  
185 calculated as the volume between the standing water surface and the maximum water boundary where water ~~may~~  
186 might overspill into downstream wetlands or waters. The potential flow paths representing surface water  
187 connectivity ~~can-were then be~~ derived according to the potential water storage and simulated rainfall intensity. The  
188 flowchart in Fig. 3 shows the detailed procedures of the methodology for delineating wetland catchments and  
189 potential flow paths.

### 190 3.2 Extraction of hierarchical wetland depressions

191 The fill-and-spill hydrology of prairie wetland depressions have received considerable attention in recent years  
192 (Shaw et al., 2012; Shaw et al., 2013; Golden et al., 2014; Chu, 2015; Hayashi et al., 2016; Wu and Lane, 2016). It  
193 is generally acknowledged that the fill-and-spill mechanism of wetland depressions results in intermittent hydrologic  
194 connectivity between wetlands in the ~~Prairie Pothole Region of North America~~PPR. In this study, wetland  
195 depressions were categorized into two groups based on their hierarchical structure: simple depressions and  
196 composite depressions. A simple depression is a depression that does not have any other depressions embedded in it,  
197 whereas a composite depression is composed of two or more simple depressions (Wu and Lane, 2016). As shown in  
198 Fig. 4(a), for example, depressions A, B, C, D and E are all simple depressions. As water level gradually increases in  
199 these simple depressions, they will eventually begin to spill and merge to form composite depressions. For instance,  
200 the two ~~adjacent-adjointing~~ simple depressions A and B can form a composite depression F (see Fig. 4(b)).  
201 Continuously, composite depression F and simple depression C can further coalesce to form an even larger  
202 composite depression G. Similarly, the two ~~adjoining adjacent~~ simple depressions D and E can coalesce to form a  
203 composite depression H.

204 It is worth noting that the flow direction of surface waters resulting from the fill-and-spill mechanism  
205 between ~~adjoining adjacent~~ wetland depressions can be bidirectional, depending on the antecedent water level and  
206 potential water storage capability of the depressions. Most previous studies simply assumed that water always flows  
207 unidirectionally from an upper waterbody to a lower one. This assumption, however, does not apply when two  
208 ~~adjoining adjacent~~ depressions share the same spilling elevation or when there is a groundwater hydraulic head  
209 preventing the flow from one to another. For example, in Fig. 4(a), the water flow direction resulting from fill-and-  
210 spill between depressions A and B can be bidirectional. If depression B fills up more quickly than depression A,  
211 then water will flow from depression B to depression A through the spilling point, and vice versa. Depression with a

212 high elevation of antecedent water level does not necessarily spill to an ~~adjoining adjacent~~ depression with a lower  
213 elevation of antecedent water level. The key factors affecting the initialization of spilling process leading to flow  
214 direction are the depression ponding time and catchment precipitation conditions. If the rain or runoff comes from  
215 the east and that is where depression B is, then it might fill more quickly than if the runoff comes from the west  
216 where depression A is. The wetland depression whichever takes less time to fill up will spill to the ~~adjoining~~  
217 ~~adjacent~~ depression and eventually coalesce to form a larger composite depression. If no ~~adjacent adjoining~~  
218 depression with the same spilling elevation is available, the upstream wetland depression will directly spill to  
219 downstream wetlands or ~~river~~ streams. For example, the largest fully-filled composite depression G will spill to the  
220 simple depression D or the composite depression H, if available.

221 To identify and delineate the nested hierarchical structure of potential wetland depressions, we utilized the  
222 localized contour tree method proposed by Wu et al. (2015). The concept of contour tree was initially proposed to  
223 extract key topographic features (e.g., peaks, pits, ravines, and ridges) from contour maps (Kweon and Kanade,  
224 1994). The contour tree is a tree data structure that can represent the nesting of contour lines on a continuous  
225 topographic surface. Wu et al. (2015) improved and implemented the contour tree algorithm, making it a locally  
226 adaptive version. In other words, the localized contour tree algorithm builds a series of trees rather than a single  
227 global contour tree for the entire area. Each localized contour tree represents one disjointed depression (simple or  
228 composite), and the number of trees represents the total number of disjointed depressions for the entire area. When a  
229 disjointed depression is fully flooded, the water in it will spill to the downstream wetlands or waters through  
230 overland flow. For example, Fig. 4(c) and (d) show the corresponding contour tree graphs for the composite  
231 depressions in Fig. 4(b). Once the composition G is fully filled, water will spill into simple depression D or  
232 composite depression H.

### 233 3.3 Delineation of nested wetland catchments

234 After the identification and extraction of hierarchical wetland depressions from the contour maps, various  
235 hydrologically relevant terrain attributes can be derived based on the DEM, including flow direction, flow  
236 accumulation, catchment boundary, flow path, flow length, etc. The calculation of flow direction is essential in  
237 hydrological analysis because it frequently serves as the first step to derive other hydrologically important terrain  
238 attributes. On a topographic surface represented in a DEM, flow direction is the direction of flow from each grid cell  
239 to its steepest downslope neighbor. One of the widely used flow direction algorithms is the eight-direction flow  
240 model known as the D8 algorithm (O'Callaghan and Mark, 1984), which is available in most GIS software packages.  
241 Flow accumulation is computed based on flow direction. Each cell value in the flow accumulation raster represents  
242 the number of upslope cells that flow into it. In general, cells with high flow accumulation values correspond to  
243 areas of concentrated flow (e.g. stream channels), while cells with a flow accumulation value of zero correspond to  
244 the pattern of ridges (Zhu, 2016). Therefore, flow accumulation provides a basis for identifying ridgelines and  
245 delineating catchment boundaries.

246 A catchment is the upslope area that drains water to a common outlet. It is also known as the watershed,  
247 drainage basin, or contributing area. Catchment boundaries can be delineated from a DEM by identifying ridgelines

248 between catchments based on a specific set of catchment outlets (i.e., spilling points). In traditional hydrological  
 249 modeling, topographic depressions are commonly treated as spurious ~~depressions (or is it “features”)~~ and simply  
 250 removed to create a hydrologically correct DEM, which enforces water to flow continuously across the landscape to  
 251 the catchment outlets (e.g., stream gauges, dams). In the PPR, however, most topographic depressions in the DEM  
 252 are real features that represent wetland depressions, which are rarely under fully-filled condition (see Hayashi et al.,  
 253 2016; Lane and D'Amico, 2016; Vanderhoof et al., 2016). As illustrated above, we used the localized contour tree  
 254 algorithm to delineate the hierarchical wetland depressions, which ~~can be used~~ used as the source locations for  
 255 delineating wetland catchments. Each wetland depression (simple or composite) has a corresponding wetland  
 256 catchment. As shown in Fig. 4(b), the corresponding wetland catchment of each wetland depression is bounded by  
 257 the vertical lines surrounding that depression. For example, the wetland catchment of simple depression A is  
 258  $Catchment_{lm}$ , and the wetland catchment of simple depression B is  $Catchment_{mn}$ . Similarly, the wetland  
 259 catchment of composite depression F is  $Catchment_{ln}$ , which is an aggregated area of  $Catchment_{lm}$  and  
 260  $Catchment_{mn}$ , resulting from the coalesce ~~from of~~ simple depressions A and B.

### 261 3.4 Calculation of potential water storage and ponding time

262 The potential water storage capacity ( $V$  [m<sup>3</sup>]) of each wetland depression ~~can be used~~ computed through statistical  
 263 analysis of the grid cells that fall within the depression (Wu and Lane, 2016):

$$264 \quad V = \sum_{i=1}^n (C - Z_i) \cdot R^2 \quad (1)$$

265 where  $C$  is the spilling elevation (m), i.e., the elevation of the grid cell where water spills out of the depression;  $Z_i$   
 266 is the elevation of the grid cell  $i$  (m);  $R$  is the spatial resolution (m); and  $n$  is the total number of grid cells that fall  
 267 within the depression.

268 The ponding time of a depression ~~can be used~~ calculated as follows:

$$269 \quad T = V / (A_c \cdot I) \cdot 1000 \quad (2)$$

270 where  $V$  is the potential water storage capacity of the depression (m<sup>3</sup>);  $A_c$  is the catchment area of the  
 271 corresponding depression (m<sup>2</sup>); and  $I$  is the rainfall intensity (mm/h). For the sake of simplicity, we made two  
 272 assumptions. First, we assumed that the rainfall ~~is was~~ temporally and spatially consistent and uniformly distributed  
 273 throughout the landscape (e.g., 50 mm/h) and all surfaces ~~are were~~ impervious. Second, we assumed no soil  
 274 infiltration. ———

275 The proportion of wetland depression area ( $A_w$ ) to catchment area ( $A_c$ ) ~~is was~~ calculated by:

$$276 \quad P_{wc} = A_w / A_c \quad (3)$$

277 The wetland depression area ( $A_w$ ) refers to the maximum ponding extent of the depression. The proportion ( $P_{wc}$ )  
278 can serve as a good indicator for percent inundation of the study area under extremely wet conditions (e.g.,  
279 Vanderhoof et al., 2016).

### 280 **3.5 Derivation of surface-water flow paths**

281 Based on the computed ponding time of each depression under a specific rainfall intensity, the most probable  
282 sequence of the overland flow path ~~can be~~ constructed. The depression with the least ponding time will first fill  
283 and start to overflow down-gradient. In hydrology, the path which water takes to travel from the spilling point to the  
284 downstream surface outlet or channel is commonly known as flow path. The distance it takes for water to travel is  
285 known as flow length. In this study, we adopted and adapted the least-cost path search algorithm (Wang and Liu,  
286 2006; Metz et al., 2011; Stein et al., 2011) to derive the potential flow paths. The least cost path algorithm requires  
287 two input datasets: the DEM and the depression polygons. Given the fact that topographic depressions in high-  
288 resolution LiDAR DEM are frequently a combination of artifacts and actual landscape features (Lindsay and Creed,  
289 2006), the user can set a minimum size threshold for depressions to be treated as actual landscape features. In other  
290 words, depressions with a size smaller than the threshold will be treated as artifacts, and thus removed from the  
291 DEM. This results in a partially-filled DEM in which depressions smaller than the chosen threshold are filled to  
292 enforce hydrologic flow while larger depressions are kept for further analysis. Based on the partially-filled DEM,  
293 flow direction for each grid cell can be calculated using the D8 flow direction algorithm (O'Callaghan and Mark,  
294 1984). The least cost path minimizes the cumulative cost (i.e., elevation) along its length. Flow paths are computed  
295 by tracing down gradient, from higher to lower cells, following assigned flow directions. With the simulated  
296 overland flow path, flow length can be calculated, which is defined as the distance between the spilling point of an  
297 upslope wetland and the inlet of a downslope wetland or stream. In our study, hydrologic connectivity refers to the  
298 water movement between wetland-wetland and wetland-stream via hydrologic pathways of surface water.

### 299 **3.6 Wetland Hydrology Analyst**

300 To facilitate automated delineation of wetland catchments and flow paths, we ~~have~~ implemented the proposed  
301 framework as an ArcGIS toolbox – Wetland Hydrology Analyst, which is freely available for download at  
302 <https://GISTools.github.io/> (accessed December 30, 2016). The core algorithms of the toolbox were implemented  
303 using the Python programming language. The toolbox consists of three tools: Wetland Depression Tool, Wetland  
304 Catchment Tool, and Flow Path Tool. The Wetland Depression Tool asks the user to select a DEM grid, and then  
305 executes the localized contour tree algorithm with user-defined parameters (e.g., base contour elevation, contour  
306 interval, min. depression size, min. ponding depth) automatically to delineate hierarchical wetland depressions. The  
307 depressional wetland polygons can be stored as ESRI Shapefiles or a Feature Dataset in a Geodatabase. Various  
308 morphometric properties (e.g., width, length, size, perimeter, max. depth, mean depth, volume, elongatedness,  
309 compactness) are computed and included in the attribute table of the wetland polygon layers. The Wetland  
310 Catchment Tool uses the DEM grid and the wetland polygon layers resulted from the Wetland Depression Tool as

input, and exports wetland catchment layers in both vector and raster format. The Flow Path Tool can be used to derive [potential](#) overland flow paths of surface water based on the DEM grid and the wetland polygon layers.

### **[3.7 Wetland inundation mapping](#)**

The LiDAR intensity image was primarily used to map inundation areas. Before inundation mapping, we applied a [median filter](#) to smooth the LiDAR intensity image. The median filter is considered as an edge-preserving filter that can effectively remove data noise while preserving boundaries between image objects (Wu et al., 2014). Subsequently, a simple thresholding method was used to separate inundated and non-inundated classes. Similar thresholding techniques have been used in previous studies to extract water areas from LiDAR intensity imagery (Lang and McCarty, 2009; Huang et al., 2011b). By examining typical inundation areas and the histogram of the LiDAR intensity imagery used in our study, we chose an intensity threshold value of 20. Grid cells with an intensity value between 0 and 20 were classified as an inundated class while grid cells with an intensity value greater than 20 as a non-inundated class, which resulted in a binary image. In the binary image, each region composed of inundated pixels that were spatially connected (8-neighbor) was referred to as a potential inundation object. The “boundary clean” and “region group” functions in ArcGIS Spatial Analyst were then used to clean ragged edges of the potential inundation objects and assign a unique number to each object. It should be noted that water and live trees might both appear as dark features in the LiDAR intensity imagery and have similar intensity values, although trees are not particularly common in this region. As a result, some trees were misclassified as inundation objects. To correct the misclassifications and obtain reliable inundation objects, we further refined the potential inundation objects using additional criteria with the aid of the LiDAR DEM. ~~First-of-all~~, we assumed that each inundation object must occur within a topographic depression in order to retain water. In other words, all inundation objects must intersect with depression objects derived using the “sink” function in ArcGIS Spatial Analyst. Secondly, given the relatively flat and level surface of inundated regions, the standard deviation of pixel elevations within the same inundation object should be very small. By examining the standard deviation of pixel elevations of some typical inundation objects and tree objects, we chose a threshold of 0.25 m, which is slightly larger than the vertical accuracy of the LiDAR data (0.15 m). This step can be achieved using the “zonal statistics as table” in ArcGIS Spatial Analyst. Thirdly, we only focused on wetlands greater than 500 m<sup>2</sup>. Therefore, inundation objects with areas smaller than 500 m<sup>2</sup> were eliminated from further analysis.

## **4 Results**

### **4.1 Inundation mapping [results](#)**

~~The LiDAR intensity image was primarily used to map inundation areas. Before inundation mapping, we applied a median filter to smooth the LiDAR intensity image. The median filter is considered as an edge-preserving filter that can effectively remove data noise while preserving boundaries between image objects (Wu et al., 2014). Subsequently, a simple thresholding method was used to separate inundated and non-inundated classes. Similar thresholding techniques have been used in previous studies to extract water areas from LiDAR intensity imagery~~

345 ([Lang and McCarty, 2009](#); [Huang et al., 2011b](#)). By examining typical inundation areas and the histogram of the  
346 LiDAR intensity imagery used in our study, we chose an intensity threshold value of 20. Grid cells with an intensity  
347 value between 0 and 20 were classified as an inundated class while grid cells with an intensity value greater than 20  
348 as a non-inundated class, which resulted in a binary image. In the binary image, each region composed of inundated  
349 pixels that were spatially connected (8-neighbor) was referred to as a potential inundation object. The “boundary  
350 clean” and “region group” functions in ArcGIS Spatial Analyst were then used to clean ragged edges of the potential  
351 inundation objects and assign a unique number to each object. It should be noted that water and live trees might both  
352 appear as dark features in the LiDAR intensity imagery and have similar intensity values, although trees are not  
353 particularly common in this region. As a result, some trees were misclassified as inundation objects. To correct the  
354 misclassifications and obtain reliable inundation objects, we further refined the potential inundation objects using  
355 additional criteria with the aid of the LiDAR DEM. First of all, we assumed that each inundation object must occur  
356 within a topographic depression in order to retain water. In other words, all inundation objects must intersect with  
357 depression objects derived using the “sink” function in ArcGIS Spatial Analyst. Secondly, given the relatively flat  
358 and level surface of inundated regions, the standard deviation of pixel elevations within the same inundation object  
359 should be very small. By examining the standard deviation of pixel elevations of some typical inundation objects  
360 and tree objects, we chose a threshold of 0.25 m, which is slightly larger than the vertical accuracy of the LiDAR  
361 data (0.15 m). This step can be achieved using the “zonal statistics as table” in ArcGIS Spatial Analyst. Thirdly, we  
362 only focused on wetlands greater than 500 m<sup>2</sup>. Therefore, inundation objects with areas smaller than 500 m<sup>2</sup> were  
363 eliminated from further analysis.

364 Using the above procedures, we identified 15,784 inundation objects (i.e., depressions  $\geq 500$  m<sup>2</sup> with water as  
365 determined through LiDAR-based analyses), which were then compared against the NWI wetland polygons in our  
366 study area. We have made the inundation map publicly available at <https://GISTools.github.io/> (accessed December  
367 30, 2016). The identified inundation objects encompassed an area of approximately 278.5 km<sup>2</sup>, accounting for 10.1 %  
368 of the Pipestem subbasin. Using the empirical area-to-volume equation developed for this region of the PPR (see  
369 Gleason et al., 2007; Wu and Lane, 2016), we estimated that the 15,784 inundated depressions stored approximately  
370 448.5 million m<sup>3</sup> of water. The histogram of inundation polygons is shown in Fig. 5(a). The median size of the  
371 inundation polygons identified using the LiDAR intensity data was ~~4828~~  $1.8 \times 10^3$  m<sup>2</sup>, which was slightly larger  
372 than the reported median size of NWI polygons (Table 2). Surprisingly Contrary to expectations, 18,957 out of  
373 32,016 NWI wetland polygons did not intersect with the inundation objects. In other words, 59.2% of the NWI  
374 wetland polygons mapped in the 1980s were found to be partly or completely dried out or destroyed did not contain  
375 visible waterbodies during the LiDAR collection period. The total area of these ‘dried’ NWI wetlands were 43.6 km<sup>2</sup>,  
376 accounting for 15.6% of the original NWI wetland areas (279.5 km<sup>2</sup>). The histogram of the ‘dried’ NWI wetlands is  
377 shown in Fig. 5(b). It is worth noting that most of these ‘dried’ NWI wetlands were relatively small with a median  
378 size of ~~4212~~  $1.2 \times 10^3$  m<sup>2</sup> (Table 2). The LiDAR intensity data were acquired in late October 2011, an extremely wet  
379 month according to the Palmer Hydrological Drought Index (Fig. 6). During this wet season, most wetlands would  
380 be expected to have abundant standing water. If no standing water could be detected in a wetland patch during this  
381 extremely wet period, it is possible that some of these small wetlands might have ~~we can safely conclude that the~~

382 ~~wetland patch had probably~~ dried out during the past ~~decades~~weeks to months, ~~although we could not infer the exact~~  
383 ~~time when it occurred~~. It is possible that land use change surrounding the 'dried' wetlands (e.g., row-cropping  
384 replacing pasture lands) may have affected their hydrology (Wright and Wimberly, 2013); water diversion via  
385 drainage or ditches could also be responsible for the lack of inundation, though we did not explore either of these  
386 potential drivers of change in this study. However, it is also likely that some of the 'dried' wetland might become  
387 wet again in the spring following snowmelt. The 'dried' NWI wetlands could also be attributed to the source of error  
388 in the original NWI data, which has a minimum mapping unit (i.e., the minimum sized wetland that can be  
389 consistently mapped) of 0.1 ha for the PPR (Tiner, 1997). Figure 5(b) shows that 37% of the 'dried' NWI polygons  
390 are smaller than the minimum mapping unit (1000 m<sup>2</sup>). This implies that these small 'dried' NWI polygons could be  
391 due to the NWI mapping error. Figure 7 illustrates the difference in shape and extent between the LiDAR-derived  
392 wetland inundation maps and the NWI wetland polygons. The areas of disagreement (discrepancy) can be partly  
393 explained by the different image acquisition dates. As mentioned earlier, the NWI maps for Pipestem subbasin of the  
394 PPR were created in the early 1980s while the LiDAR data were acquired in 2011. Clearly, most small NWI  
395 wetlands (see ~~blue~~yellow-outline polygons in Fig. 7) appeared to not have visible standing water. Conversely, large  
396 NWI wetlands exhibited expansion and coalesced to form even large wetland complexes (see ~~yellow~~blue-outline  
397 polygons in Fig. 7).

#### 398 4.2 Nested wetland depressions and catchments

399 We applied the localized contour method on the LiDAR-derived DEM and identified 33,241 wetland depressions. It  
400 should be noted that the 'wetland depression' refers to the maximum potential ponding extent of the depression. The  
401 inundated wetland depressions identified in the prior section can be seen as a subset of these depressions with water  
402 in them. The total area of the identified wetland depressions was approximately ~~554.5~~  $0.55 \times 10^9$  km<sup>2</sup> (Table 3),  
403 accounting for 20% of the entire study area. This histogram of the wetland depressions is shown in Fig. 8(a). The  
404 median size of wetland depressions was ~~2592~~  $2.6 \times 10^3$  m<sup>2</sup>, which is larger than that of the NWI wetland polygons  
405 as well as the inundation polygons (see Table 2). Using Eq. (1), we estimated that the potential water storage  
406 capacity of the Pipestem subbasin resulting from these wetland depressions is 782.8 million m<sup>3</sup>, which is 1.75 times  
407 as large as the estimated existing water storage (448.5 million m<sup>3</sup>) for the 15,784 inundated wetlands mentioned  
408 above. As noted by Hayashi et al. (2016), wetlands and catchments are highly correlated and should be considered  
409 as integrated hydrological units. The water input of each wetland largely depends on runoff from the upland areas  
410 within the catchment. Using the method described in Section 3.3, we delineated the associated wetland catchments  
411 for each of the 33,241 wetland depressions. The histogram of the delineated wetland catchments is shown in Fig.  
412 8(b). The median size of wetland catchments was ~~25,780~~  $26 \times 10^3$  m<sup>2</sup>, which is approximately ten times larger than  
413 that of the wetland depressions (Table 3).

414 Using Eq. (3), we calculated the proportion of depression area to catchment area ( $A_w / A_c$ ) for each wetland  
415 depression. It was found that the proportion ranged from 0.04% to 83.72%, with a median of 14.31% (Table 3). Our  
416 findings are in general agreement with previous studies (Hayashi et al., 2016). For instance, Hayashi et al. (1998)

417 reported an average proportion ( $A_w/A_c$ ) of 9% for 12 prairie wetlands in the Canadian portion of the PPR.  
418 Similarly, Watmough and Schmoll (2007) analyzed 13 wetlands in the Cottonwood Lake Area during the high-stage  
419 period and reported an average proportion ( $A_w/A_c$ ) of 18%. It should be noted that the average proportion of  
420 wetland area to catchment area ( $A_w/A_c$ ) reported in the above studies were calculated on the basis of a limited  
421 number of wetlands. On the contrary, our results were computed from more than 30,000 wetland depressions and  
422 catchments, which provides a statistically reliable result [for the study area](#) due to a much larger sample size.

### 423 **4.3 [Potential Flow paths and connectivity lengths](#)**

424 Based on the LiDAR DEM and wetland depression polygon layer, we derived the [complete-potential](#) flow path  
425 network for our study area using the least-cost path algorithm. We have made the interactive map of [modeled](#)  
426 hydrologic connectivity in the Pipestem subbasin publicly available at [https://GISTools.github.io/wetland-](https://GISTools.github.io/wetland-connectivity/)  
427 [connectivity](#) (accessed December 30, 2016). A number of data layers derived from our study are available on the  
428 map, such as the inundation polygons, wetland depressions, wetland catchments, and [potential](#) flow paths. NWI  
429 polygons, NHD flowlines, LiDAR intensity image, LiDAR shaded relief, and time-series aerial photographs are also  
430 available for results comparison and visualization. A small portion of the map is shown in Fig. 9. Clearly, the  
431 derived [potential](#) flow paths not only captured the permanent surface water flow paths (see the thick blue NHD  
432 flowline in Fig. 9), but also the [potential](#) intermittent and infrequent flow paths that have not been mapped  
433 previously. By examining the potential flow paths overlaid on the color infrared aerial photograph (Fig. 9(b)), we  
434 can see that the majority of [potential](#) flow paths appeared to be collocated with vegetated areas. This indicates that  
435 flow paths are likely located in high soil moisture areas that are directly or indirectly related to surface water or  
436 groundwater connectivity. [It should be noted/reiterated that the derived flow paths are only potential flow paths.](#)  
437 [Water may not have flowed along a fraction of them to date.](#)

438 In total, there are 1840 NHD flowlines in the Pipestem subbasin. The mean and median length of NHD  
439 flowlines are 762 m and 316 m, respectively (Table 4). However, the [potential](#) flow lengths derived from our study,  
440 which connected not only stream segments but also wetlands to wetlands, revealed much shorter flow paths than the  
441 NHD flowlines. This finding is within our expectation. The histogram of the derived [potential](#) flow lengths is shown  
442 in Fig. 10. The median [potential](#) flow length is 83 m, which is approximately 1/4 of the median NHD flowlines. The  
443 median elevation difference between an upstream wetland and a downstream wetland connected through the  
444 [potential](#) flow path is 0.89 m.

## 445 **5 Discussion**

446 ~~It should be noted that~~ The LiDAR data we used in this study were collected in ~~the~~ late October ~~of~~ 2011, which was  
447 an extremely wet period according to the Palmer Hydrological Drought Index (see Fig. 6). ~~During such a wet period,~~  
448 ~~most~~ Most wetlands exhibited high water levels and large water extents, which can be evidenced from the LiDAR  
449 intensity image in Fig. 7 and the aerial photograph in Fig. 9. It can be clearly seen that most wetlands, particularly  
450 those larger ones, appeared to have larger water extents compared to the NWI polygons. A substantial number of



451 ~~inundated~~ NWI wetlands were found ~~inundated~~ to coalesce with ~~adjacent-adjoining~~ LiDAR-based wetland  
452 depressions and form larger wetland complexes. LiDAR data acquired during high water levels is desirable for  
453 studying maximum water extents of prairie wetlands. However, the use of wet-period LiDAR data alone is not ideal  
454 for studying the fill-and-spill hydrology of prairie wetlands. Since LiDAR sensors working in the near-infrared  
455 spectrum typically could not penetrate water, it is impractical to derive ~~bathymetric-bathymetry information~~ of the  
456 wetland depressions. As a result, the delineation and characterization of individual wetland depressions nested  
457 within larger inundated wetland complexes were not possible. Bathymetric LiDAR systems with a green laser  
458 onboard offer a promising solution for acquiring wetland basin morphometry due to the higher penetration capability  
459 of the green laser (Wang and Philpot, 2007). In addition, the derivation of antecedent water depth and volume of  
460 wetland depressions is difficult, which can only be estimated using empirical equations based on the statistical  
461 relationship between depression area and depression volume (Hayashi and Van der Kamp, 2000; Gleason et al.,  
462 2007). As noted earlier, the volume of water in the 15,784 inundated wetlands was estimated to be 448.5 million m<sup>3</sup>.  
463 Ideally, using multiple LiDAR datasets acquired in both dry and deluge conditions in conjunction with time-series  
464 aerial photographs would be essential for studying the fill-and-spill mechanism of prairie wetlands. In this case, we  
465 ~~can~~ could use the dry-period LiDAR data to delineate and characterize the morphology of individual wetland  
466 depressions before the fill-and-spill processes occur. Furthermore, we can derive the potential flow paths and project  
467 the coalescing of wetland depressions after the fill-and-spill processes initiate. The wet-period LiDAR data and  
468 time-series aerial photographs can serve as validation datasets to evaluate the fill-and-spill patterns.

469 It is also worth noting that the proposed methodology in this study was designed to reflect the topography  
470 and hydrologic connectivity between wetlands in the Prairie Pothole Region. We have made assumptions to simplify  
471 the complex prairie hydrology. Physically-based hydrological models (e.g., Brunner and Simmons, 2012; Ameli and  
472 Creed, 2017) have not yet been integrated into our framework. However, fill-and-spill is a complex and spatially  
473 distributed hydrological process highly affected by many factors, such as surface topography, surface roughness, soil  
474 infiltration, soil properties, depression storage, precipitation, evapotranspiration, snowmelt runoff, and groundwater  
475 exchange (Tromp-van Meerveld and McDonnell, 2006b, a; Evenson et al., 2015; Zhao and Wu, 2015; Evenson et  
476 al., 2016; Hayashi et al., 2016). Nevertheless, our study presents the first attempt to use LiDAR data for deriving  
477 nested wetland catchments and simulating flow paths in the broad-scale Pipestem subbasin in the PPR. Previous  
478 studies utilizing high-resolution digital elevation data (e.g., LiDAR, Interferometric Synthetic Aperture Radar  
479 [IfSAR]) for studying prairie wetlands were mostly confined in small-scale areas (e.g., plot scale, small watershed  
480 scale) with a limited number of wetlands, whereas broad-scale studies using physically-based hydrological models  
481 have rarely used LiDAR data to delineate and characterize individual wetland depressions or catchments. Coupled  
482 surface-subsurface flow models with hydrologic, biogeochemical, ecologic, and geographic perspectives have yet to  
483 be developed for broad-scale studies in the PPR (Golden et al., 2014; Amado et al., 2016). Further efforts are still  
484 needed to improve the understanding of the integrated surface-water and groundwater processes of prairie wetlands.

## 485 **6 Conclusions**

486 Accurate delineation and characterization of wetland depressions and catchments are essential to understand and  
487 correctly analyze the hydrology of many landscapes, including the Prairie Pothole Region. ~~for understanding the~~  
488 ~~hydrology of prairie wetlands.~~ In this study, we accurately delineated the inundation areas while reducing the  
489 confounding factor of live trees by using the LiDAR-derived DEM in conjunction with the coincident LiDAR  
490 intensity imagery. In addition, we developed a semi-automated framework for identifying nested hierarchical  
491 wetland depressions and delineating their corresponding catchments using the localized contour tree method.  
492 Furthermore, we quantified the potential hydrologic connectivity between wetlands and streams based on the  
493 overland flow networks derived using the least-cost path algorithm on LiDAR data. Although the results presented  
494 in this study are specific to the Pipestem subbasin, the proposed framework can be easily adopted and adapted to  
495 other ~~PPR regions, as well as other~~ wetland regions where ~~fine resolution~~-LiDAR data are available. The new tools  
496 that we developed and have made freely available to the scientific community for identifying potential hydrologic  
497 connectivity between wetlands and stream networks can better inform ~~wetland regulation debates regulatory~~  
498 ~~decisions~~ and enhance the ability to better manage wetlands under various planning scenarios. The resulting flow  
499 network delineated ~~putative temporary or seasonal~~potential flow paths connecting wetland depressions to each other  
500 or to the river network at scales finer than available through the National Hydrography Dataset. The results  
501 demonstrated that our proposed framework is promising for improving overland flow modeling and hydrologic  
502 connectivity analysis (Golden et al., 2016).

503 Broad-scale prairie wetland hydrology has been difficult to study with traditional remote sensing methods  
504 using multi-spectral satellite data due to the limited spatial resolution and the interference of tree canopy (Klemas,  
505 2011; Gallant, 2015). LiDAR-derived DEMs can be used to map potential hydrologic flow pathways, which regulate  
506 the ability of wetlands to provide ecosystem services (Lang and McCarty, 2009). This study is an initial step towards  
507 the development of a spatially distributed hydrologic model to fully describe the hydrologic processes in broad-scale  
508 prairie wetlands. Additional field work and the integration of physically-based models of surface and subsurface  
509 processes would benefit the study. Importantly, the results capture temporary and ephemeral hydrologic connections  
510 and provide essential information for wetland scientists and decision-makers to more effectively plan for current and  
511 future management of prairie wetlands.

512

513 **Data and code availability**

514 The data and ArcGIS toolbox developed for this paper are available for download at <https://GISTools.github.io/>.

515 **Competing interests**

516 The authors declare that they have no conflict of interest.

517 **Disclaimer/Acknowledgements**

518 [The authors would like to thank Rose Kwok, Daniel Auerbach, and two anonymous journal reviewers for providing](#)  
519 [insightful comments which improved the quality of the manuscript.](#) This paper has been reviewed in accordance  
520 with the U.S. Environmental Protection Agency's peer and administrative review policies and approved for  
521 publication. Mention of trade names or commercial products does not constitute endorsement or recommendation  
522 for use. Statements in this publication reflect the authors' professional views and opinions and should not be  
523 construed to represent any determination or policy of the U.S. Environmental Protection Agency.

525 **References**

- 526 Amado, A. A., Politano, M., Schilling, K., and Weber, L.: Investigating Hydrologic Connectivity of a Drained  
527 Prairie Pothole Region Wetland Complex using a Fully Integrated, Physically-Based Model, *Wetlands*, 1-13,  
528 10.1007/s13157-016-0800-5, 2016.
- 529 Ameli, A. A., and Creed, I. F.: Quantifying hydrologic connectivity of wetlands to surface water systems, *Hydrol.*  
530 *Earth Syst. Sci.*, 21, 1791-1808, 10.5194/hess-21-1791-2017, 2017.
- 531 Bengtson, M. L., and Padmanabhan, G.: A hydrologic model for assessing the influence of wetlands on flood  
532 hydrographs in the Red River Basin: Development and application, Citeseer, 1999.
- 533 Brunner, P., and Simmons, C. T.: HydroGeoSphere: A Fully Integrated, Physically Based Hydrological Model,  
534 *Ground Water*, 50, 170-176, 10.1111/j.1745-6584.2011.00882.x, 2012.
- 535 Chu, X.: Delineation of Pothole-Dominated Wetlands and Modeling of Their Threshold Behaviors, *Journal of*  
536 *Hydrologic Engineering*, D5015003, 2015.
- 537 Cohen, M. J., Creed, I. F., Alexander, L., Basu, N. B., Calhoun, A. J., Craft, C., D'Amico, E., DeKeyser, E., Fowler,  
538 L., and Golden, H. E.: Do geographically isolated wetlands influence landscape functions?, *Proceedings of*  
539 *the National Academy of Sciences*, 113, 1978-1986, 2016.
- 540 Cowardin, L. M., Carter, V., Golet, F. C., and LaRoe, E. T.: Classification of wetlands and deepwater habitats of the  
541 United States, U.S. Department of the Interior, Fish and Wildlife Service, Washington, D.C., 131, 1979.
- 542 Dahl, T. E.: Wetlands losses in the United States, 1780's to 1980's. Report to the Congress, U.S. Department of the  
543 Interior, Fish and Wildlife Service, Washington, D.C., 13, 1990.
- 544 Dahl, T. E.: Status and trends of prairie wetlands in the United States 1997 to 2009, U.S. Department of the Interior,  
545 Fish and Wildlife Service, Ecological Services, Washington, D.C., 67, 2014.
- 546 Evenson, G. R., Golden, H. E., Lane, C. R., and D'Amico, E.: Geographically isolated wetlands and watershed  
547 hydrology: A modified model analysis, *Journal of Hydrology*, 529, Part 1, 240-256,  
548 <http://dx.doi.org/10.1016/j.jhydrol.2015.07.039>, 2015.
- 549 Evenson, G. R., Golden, H. E., Lane, C. R., and D'Amico, E.: An improved representation of geographically isolated  
550 wetlands in a watershed-scale hydrologic model, *Hydrological Processes*, 30, 4168-4184,  
551 10.1002/hyp.10930, 2016.
- 552 Gallant, A.: The Challenges of Remote Monitoring of Wetlands, *Remote Sensing*, 7, 10938, 2015.

553 Gleason, R. A., Tangen, B. A., Laubhan, M. K., Kermes, K. E., and Euliss Jr, N. H.: Estimating water storage  
554 capacity of existing and potentially restorable wetland depressions in a subbasin of the Red River of the  
555 North, U.S. Geological Survey Open-File Report 2007-1159., 36, 2007.

556 Gleason, R. A., Laubhan, M. K., Tangen, B. A., and Kermes, K. E.: Ecosystem services derived from wetland  
557 conservation practices in the United States Prairie Pothole Region with an emphasis on the US Department  
558 of Agriculture Conservation Reserve and Wetlands Reserve Programs, 2008.

559 Golden, H. E., Lane, C. R., Amatya, D. M., Bandilla, K. W., Kiperwas, H. R., Knightes, C. D., and Ssegane, H.:  
560 Hydrologic connectivity between geographically isolated wetlands and surface water systems: A review of  
561 select modeling methods, *Environ. Modell. Softw.*, 53, 190-206, 10.1016/j.envsoft.2013.12.004, 2014.

562 Golden, H. E., Creed, I., Ali, G., Basu, N., Neff, B., Rains, M., McLaughlin, D., Alexander, L., Ameli, A.,  
563 Christensen, J., Evenson, G., Jones, C., Lane, C., and Lang, M.: Scientific tools for integrating  
564 geographically isolated wetlands into land management decisions, *Frontiers in Ecology and the Environment*  
565 (in review), 2016.

566 Hayashi, M., van der Kamp, G., and Rudolph, D. L.: Water and solute transfer between a prairie wetland and  
567 adjacent uplands, 1. Water balance, *Journal of Hydrology*, 207, 42-55, [http://dx.doi.org/10.1016/S0022-  
568 1694\(98\)00098-5](http://dx.doi.org/10.1016/S0022-1694(98)00098-5), 1998.

569 Hayashi, M., and Van der Kamp, G.: Simple equations to represent the volume–area–depth relations of shallow  
570 wetlands in small topographic depressions, *Journal of Hydrology*, 237, 74-85, 2000.

571 Hayashi, M., van der Kamp, G., and Rosenberry, D. O.: Hydrology of Prairie Wetlands: Understanding the  
572 Integrated Surface-Water and Groundwater Processes, *Wetlands*, 1-18, 10.1007/s13157-016-0797-9, 2016.

573 Huang, C., Peng, Y., Lang, M., Yeo, I. Y., and McCarty, G.: Wetland inundation mapping and change monitoring  
574 using Landsat and airborne LiDAR data, *Remote Sensing of Environment*, 141, 231-242, 2014.

575 Huang, S., Dahal, D., Young, C., Chander, G., and Liu, S.: Integration of Palmer Drought Severity Index and remote  
576 sensing data to simulate wetland water surface from 1910 to 2009 in Cottonwood Lake area, North Dakota,  
577 *Remote Sensing of Environment*, 115, 3377-3389, 2011a.

578 Huang, S., Young, C., Feng, M., Heidemann, K., Cushing, M., Mushet, D. M., and Liu, S.: Demonstration of a  
579 conceptual model for using LiDAR to improve the estimation of floodwater mitigation potential of Prairie  
580 Pothole Region wetlands, *Journal of Hydrology*, 405, 417-426, 2011b.

581 Hubbard, D. E., and Linder, R. L.: Spring runoff retention in prairie pothole wetlands, *Journal of Soil & Water  
582 Conservation*, 41, 122-125, 1986.

583 Jin, S., Yang, L., Danielson, P., Homer, C., Fry, J., and Xian, G.: A comprehensive change detection method for  
584 updating the national land cover database to circa 2011, *Remote Sensing of Environment*, 132, 159-175,  
585 2013.

586 Johnston, C. A.: Wetland losses due to row crop expansion in the dakota prairie pothole region, *Wetlands*, 33, 175-  
587 182, 10.1007/s13157-012-0365-x, 2013.

588 Keddy, P. A.: *Wetland ecology: principles and conservation*, Cambridge University Press, 2010.

589 Klemas, V.: Remote sensing of wetlands: case studies comparing practical techniques, *Journal of Coastal Research*,  
590 27, 418-427, 2011.

591 Kweon, I. S., and Kanade, T.: Extracting topographic terrain features from elevation maps, *CVGIP: Image  
592 Understanding*, 59, 171-182, 10.1006/ciun.1994.1011, 1994.

593 Lane, C. R., and D'Amico, E.: Identification of Putative Geographically Isolated Wetlands of the Conterminous  
594 United States, *JAWRA Journal of the American Water Resources Association*, n/a-n/a, 10.1111/1752-  
595 1688.12421, 2016.

596 Lang, M., and McCarty, G.: Lidar intensity for improved detection of inundation below the forest canopy, *Wetlands*,  
597 29, 1166-1178, 10.1672/08-197.1, 2009.

598 Lindsay, J. B., and Creed, I. F.: Distinguishing actual and artefact depressions in digital elevation data, *Computers  
599 and Geosciences*, 32, 1192-1204, 10.1016/j.cageo.2005.11.002, 2006.

600 McCauley, L., and Anteau, M.: Generating Nested Wetland Catchments with Readily-Available Digital Elevation  
601 Data May Improve Evaluations of Land-Use Change on Wetlands, *Wetlands*, 1-10, 10.1007/s13157-014-  
602 0571-9, 2014.

603 Metz, M., Mitasova, H., and Harmon, R.: Efficient extraction of drainage networks from massive, radar-based  
604 elevation models with least cost path search, *Hydrology and Earth System Sciences*, 15, 667-678, 2011.

605 Miller, M. W., and Nudds, T. D.: Prairie landscape change and flooding in the Mississippi River Valley,  
606 *Conservation Biology*, 10, 847-853, 1996.

607 Minke, A. G. N.: Estimating water storage of prairie pothole wetlands, University of Saskatchewan, 2009.

608 Mushet, D. M., and Euliss, N. H.: The Cottonwood Lake study area, a long-term wetland ecosystem monitoring site,  
609 US Geological Survey 2327-6932, 2012.

610 Mushet, D. M., Calhoun, A. J., Alexander, L. C., Cohen, M. J., DeKeyser, E. S., Fowler, L., Lane, C. R., Lang, M.  
611 W., Rains, M. C., and Walls, S. C.: Geographically isolated wetlands: rethinking a misnomer, *Wetlands*, 35,  
612 423-431, 2015.

613 O'Callaghan, J. F., and Mark, D. M.: The extraction of drainage networks from digital elevation data, *Computer  
614 vision, graphics, and image processing*, 28, 323-344, 1984.

615 Oslund, F. T., Johnson, R. R., and Hertel, D. R.: Assessing Wetland Changes in the Prairie Pothole Region of  
616 Minnesota From 1980 to 2007, *Journal of Fish and Wildlife Management*, 1, 131-135, 10.3996/122009-  
617 JFWM-027, 2010.

618 Rover, J., and Mushet, D. M.: 16 Mapping Wetlands and Surface Water in the Prairie Pothole Region of North  
619 America, *Remote Sensing of Wetlands: Applications and Advances*, 347, 2015.

620 Shaw, D. A., Vanderkamp, G., Conly, F. M., Pietroniro, A., and Martz, L.: The fill-spill hydrology of Prairie  
621 wetland complexes during drought and deluge, *Hydrological Processes*, 26, 3147-3156, 2012.

622 Shaw, D. A., Pietroniro, A., and Martz, L.: Topographic analysis for the prairie pothole region of Western Canada,  
623 *Hydrological Processes*, 27, 3105-3114, 2013.

624 Sloan, C. E.: Ground-water hydrology of prairie potholes in North Dakota, Professional Paper 585-C, U.S.  
625 Government Printing Office Washington, D.C., USA, 1972.

626 Stanislawski, L. V.: Feature pruning by upstream drainage area to support automated generalization of the United  
627 States National Hydrography Dataset, *Computers, Environment and Urban Systems*, 33, 325-333,  
628 <http://dx.doi.org/10.1016/j.compenvurbsys.2009.07.004>, 2009.

629 Steen, V., Skagen, S. K., and Noon, B. R.: Vulnerability of Breeding Waterbirds to Climate Change in the Prairie  
630 Pothole Region, U.S.A, *PLoS ONE*, 9, e96747, 10.1371/journal.pone.0096747, 2014.

631 Stein, A., Pebesma, E., Heuvelink, G., Melles, S. J., Jones, N. E., Schmidt, B., and Rayfield, B.: Spatial Statistics  
632 2011: Mapping Global Change A least-cost path approach to stream delineation using lakes as patches and a  
633 digital elevation model as the cost surface, *Procedia Environmental Sciences*, 7, 240-245,  
634 <http://dx.doi.org/10.1016/j.proenv.2011.07.042>, 2011.

635 Tiner, R.: Geographically isolated wetlands of the United States, *Wetlands*, 23, 494-516, 10.1672/0277-  
636 5212(2003)023[0494:GIWOTU]2.0.CO;2, 2003.

637 Tiner, R. W.: NWI maps: what they tell us, *National Wetlands Newsletter*, 19, 7-12, 1997.

638 Todhunter, P. E., and Rundquist, B. C.: Terminal lake flooding and wetland expansion in Nelson County, North  
639 Dakota, *Phys. Geogr.*, 25, 68-85, 2004.

640 Tromp-van Meerveld, H. J., and McDonnell, J. J.: Threshold relations in subsurface stormflow: 1. A 147-storm  
641 analysis of the Panola hillslope, *Water Resources Research*, 42, n/a-n/a, 10.1029/2004WR003778, 2006a.

642 Tromp-van Meerveld, H. J., and McDonnell, J. J.: Threshold relations in subsurface stormflow: 2. The fill and spill  
643 hypothesis, *Water Resources Research*, 42, n/a-n/a, 10.1029/2004WR003800, 2006b.

644 U.S. EPA: Connectivity and effects of streams and wetlands on downstream waters: A review and synthesis of the  
645 scientific evidence, U.S. Environmental Protection Agency, Washington, D.C., 2015.

646 Vanderhoof, M., Alexander, L., and Todd, M. J.: Temporal and spatial patterns of wetland extent influence  
647 variability of surface water connectivity in the Prairie Pothole Region, United States, *Landscape Ecology*,  
648 31, 805-824, 10.1007/s10980-015-0290-5, 2016.

649 Vanderhoof, M., Distler, H., Mendiola, D., and Lang, M.: Integrating Radarsat-2, Lidar, and Worldview-3 Imagery  
650 to Maximize Detection of Forested Inundation Extent in the Delmarva Peninsula, USA, *Remote Sensing*, 9,  
651 105, 2017.

652 Wang, C.-K., and Philpot, W. D.: Using airborne bathymetric lidar to detect bottom type variation in shallow waters,  
653 *Remote Sensing of Environment*, 106, 123-135, 2007.

654 Wang, L., and Liu, H.: An efficient method for identifying and filling surface depressions in digital elevation models  
655 for hydrologic analysis and modelling, *International Journal of Geographical Information Science*, 20, 193-  
656 213, 2006.

657 Watmough, M. D., and Schmoll, M. J.: Environment Canada's Prairie & Northern Region Habitat Monitoring  
658 Program, Phase II: Recent Habitat Trends in the Prairie Habitat Joint Venture, Canadian Wildlife Service,  
659 2007.

660 Winter, T.: Hydrologic studies of wetlands in the northern prairie, in: Northern Prairie Wetlands, edited by: Van Der  
661 Valk, A. G., Iowa-State University Press, Ames, IA, 1989.

662 Winter, T. C., and Rosenberry, D. O.: The interaction of ground water with prairie pothole wetlands in the  
663 Cottonwood Lake area, east-central North Dakota, 1979-1990, *Wetlands*, 15, 193-211, 1995.

664 Wright, C. K., and Wimberly, M. C.: Recent land use change in the Western Corn Belt threatens grasslands and  
665 wetlands, *Proceedings of the National Academy of Sciences*, 110, 4134-4139, 2013.

666 Wu, Q., Lane, C., and Liu, H.: An Effective Method for Detecting Potential Woodland Vernal Pools Using High-  
667 Resolution LiDAR Data and Aerial Imagery, *Remote Sensing*, 6, 11444-11467, 10.3390/rs61111444, 2014.

668 Wu, Q., Liu, H., Wang, S., Yu, B., Beck, R., and Hinkel, K.: A localized contour tree method for deriving geometric  
669 and topological properties of complex surface depressions based on high-resolution topographical data,  
670 *International Journal of Geographical Information Science*, 29, 2041-2060,  
671 10.1080/13658816.2015.1038719, 2015.

672 Wu, Q., and Lane, C. R.: Delineation and Quantification of Wetland Depressions in the Prairie Pothole Region of  
673 North Dakota, *Wetlands*, 36, 215-227, 10.1007/s13157-015-0731-6, 2016.

674 Zhang, B., Schwartz, F. W., and Liu, G.: Systematics in the size structure of prairie pothole lakes through drought  
675 and deluge, *Water Resources Research*, 45, 2009.

676 Zhao, L., and Wu, F.: Simulation of Runoff Hydrograph on Soil Surfaces with Different Microtopography Using a  
677 Travel Time Method at the Plot Scale, *PloS one*, 10, e0130794, 2015.

678 Zhu, X.: *GIS for Environmental Applications: A Practical Approach*, Routledge, 2016.

679

680 **Table 1.** Summary statistics of the National Wetlands Inventory (NWI) for the Pipestem subbasin, North Dakota.

<b>Wetland type</b>	<b>Count</b>	<b>Min (m<sup>2</sup>)</b>	<b>Max (m<sup>2</sup>)</b>	<b>Median (m<sup>2</sup>)</b>	<b>Sum (m<sup>2</sup>)</b>	<b>Percentage</b>
Freshwater Emergent Wetland	31,046	500	3,105,826	1,770	241,733,542	86.5%
Freshwater Forested/ Shrub Wetland	108	548	343,950	2,572	1,175,739	0.4%
Freshwater Pond	760	533	719,339	1,772	14,719,510	5.3%
Lake	50	3,746	9,410,427	188,600	21,055,438	7.5%
Riverine	52	634	429,838	4,021	811,488	0.3%
Total (all polygons)	32,016	500	9,410,427	1,778	279,495,717	100.0%

681

<b>Wetland type</b>	<b>Count</b>	<b>Min (10<sup>3</sup> m<sup>2</sup>)</b>	<b>Max (10<sup>6</sup> m<sup>2</sup>)</b>	<b>Median (10<sup>3</sup> m<sup>2</sup>)</b>	<b>Sum (10<sup>6</sup> m<sup>2</sup>)</b>	<b>Percentage (%)</b>
Freshwater Emergent Wetland	31,046	0.50	3.1	1.8	241.7	86.5
Freshwater Forested/ Shrub Wetland	108	0.55	0.34	2.6	1.18	0.4
Freshwater Pond	760	0.53	0.72	1.8	14.7	5.3
Lake	50	3.7	9.4	188.6	21.1	7.5
Riverine	52	0.63	0.43	4.0	0.81	0.3
Total (all polygons)	32,016	0.50	9.4	1.8	279.5	100.0

682





684 **Table 2.** Summary statistics of NWI wetland polygons and inundation polygons derived from LiDAR intensity data.

<b>Type</b>	<b>Count</b>	<b>Min (m<sup>2</sup>)</b>	<b>Max (m<sup>2</sup>)</b>	<b>Mean (m<sup>2</sup>)</b>	<b>Median (m<sup>2</sup>)</b>	<b>Sum (m<sup>2</sup>)</b>
NWI polygons	32,016	500	9,410,427	8,728	1,778	279,495,717
Inundation polygons	15,784	500	7,348,000	17,650	1,825	278,523,863
Dried NWI polygons	18,957	500	112,100	2,299	1,212	43,574,627

<b>Type</b>	<b>Count</b>	<b><u>Min</u> (10<sup>3</sup> m<sup>2</sup>)</b>	<b><u>Max</u> (10<sup>6</sup> m<sup>2</sup>)</b>	<b><u>Mean</u> (10<sup>3</sup> m<sup>2</sup>)</b>	<b><u>Median</u> (10<sup>3</sup> m<sup>2</sup>)</b>	<b><u>Sum</u> (10<sup>6</sup> m<sup>2</sup>)</b>
NWI polygons	32,016	0.50	9.4	8.7	1.8	279.5
Inundation polygons	15,784	0.50	7.3	17.7	1.8	278.5
Dried NWI polygons	18,957	0.50	0.11	2.3	1.2	43.6

685

686

687 **Table 3.** Summary statistics of 33,241 wetland depressions and catchments derived from LiDAR DEM.

<b>Type</b>	<b>Min</b>	<b>Max</b>	<b>Mean</b>	<b>Median</b>	<b>Sum</b>
Depression area (m <sup>2</sup> )	1008	20,030,000	16,590	2592	554,506,299
Catchment area (m <sup>2</sup> )	1818	57,900,000	82,710	25,780	2,770,116,549
Depression volume (m <sup>3</sup> )	1	153,000,000	23,420	420	782,886,383
Proportion of depression area to catchment area (%)	0.04	83.72	16.59	14.31	20.06

688

<b>Type</b>	<b>Min</b>	<b>Max</b>	<b>Mean</b>	<b>Median</b>	<b>Sum</b>
Depression area (m <sup>2</sup> )	$1.0 \times 10^3$	$20.0 \times 10^6$	$16.6 \times 10^3$	$2.6 \times 10^3$	$0.55 \times 10^9$
Catchment area (m <sup>2</sup> )	$1.8 \times 10^3$	$57.9 \times 10^6$	$82.7 \times 10^3$	$26 \times 10^3$	$2.77 \times 10^9$
Depression volume (m <sup>3</sup> )	1	$153 \times 10^6$	$23.4 \times 10^3$	$0.42 \times 10^3$	$0.78 \times 10^9$
Proportion of depression area to catchment area (%)	0.04	83.72	16.59	14.31	20.06

689

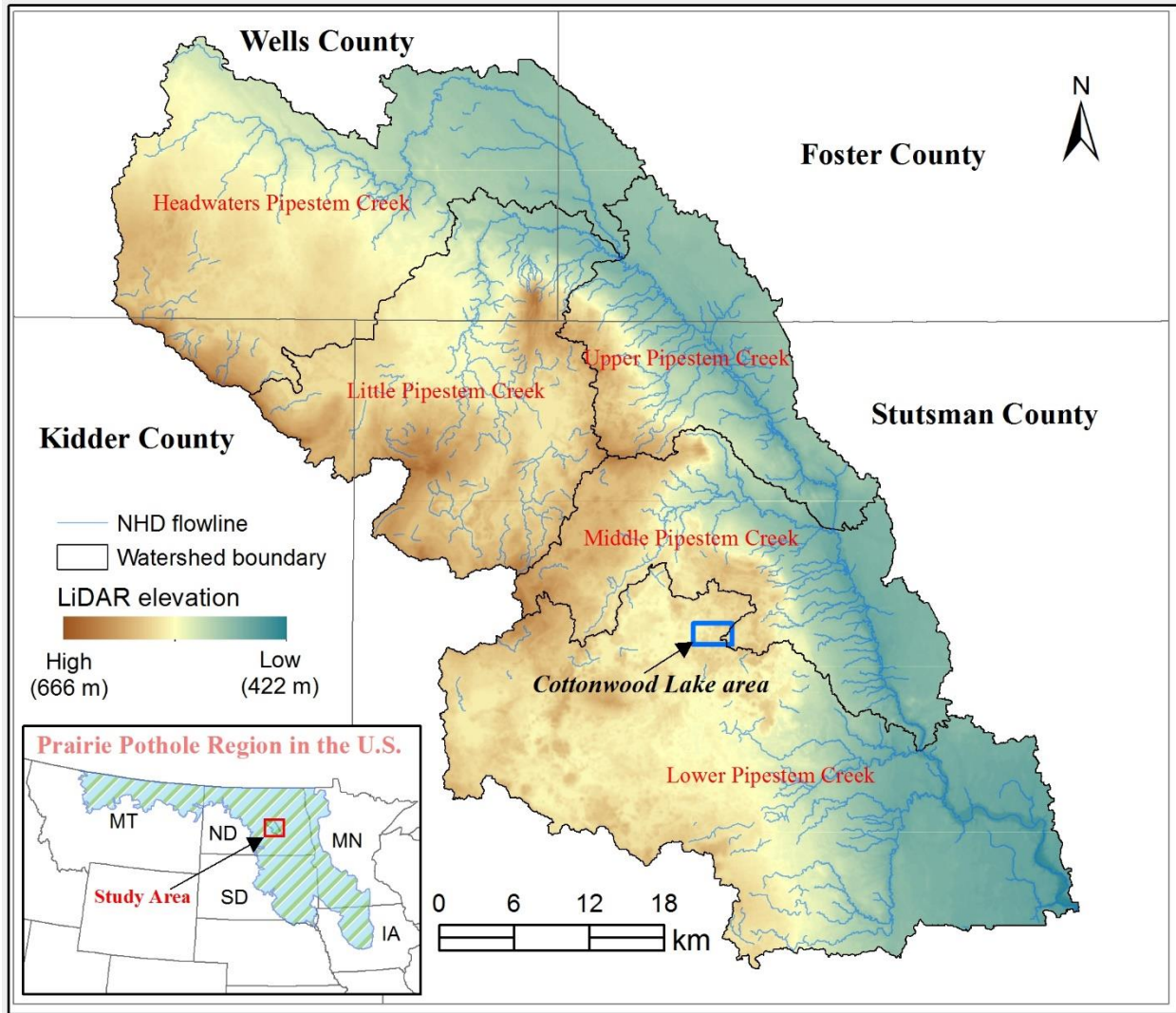
690 **Table 4.** Summary statistics of wetland depression ponding depth, NHD flowlines, ~~connectivity-flow path~~ length,  
 691 and elevation difference.

<b>Type</b>	<b>Count</b>	<b>Min (m)</b>	<b>Max (m)</b>	<b>Mean (m)</b>	<b>Median (m)</b>	<b>Sum (m)</b>
Ponding depth	33,241	0.01	7.64	0.23	0.16	NA
NHD flowlines	1840	3.89	15,530	762	317	1,402,226
Connectivity length	41,449	1.5	4,658	138	83	5,014,495
Elevation difference	41,449	0.01	70.89	2.14	0.89	NA

692

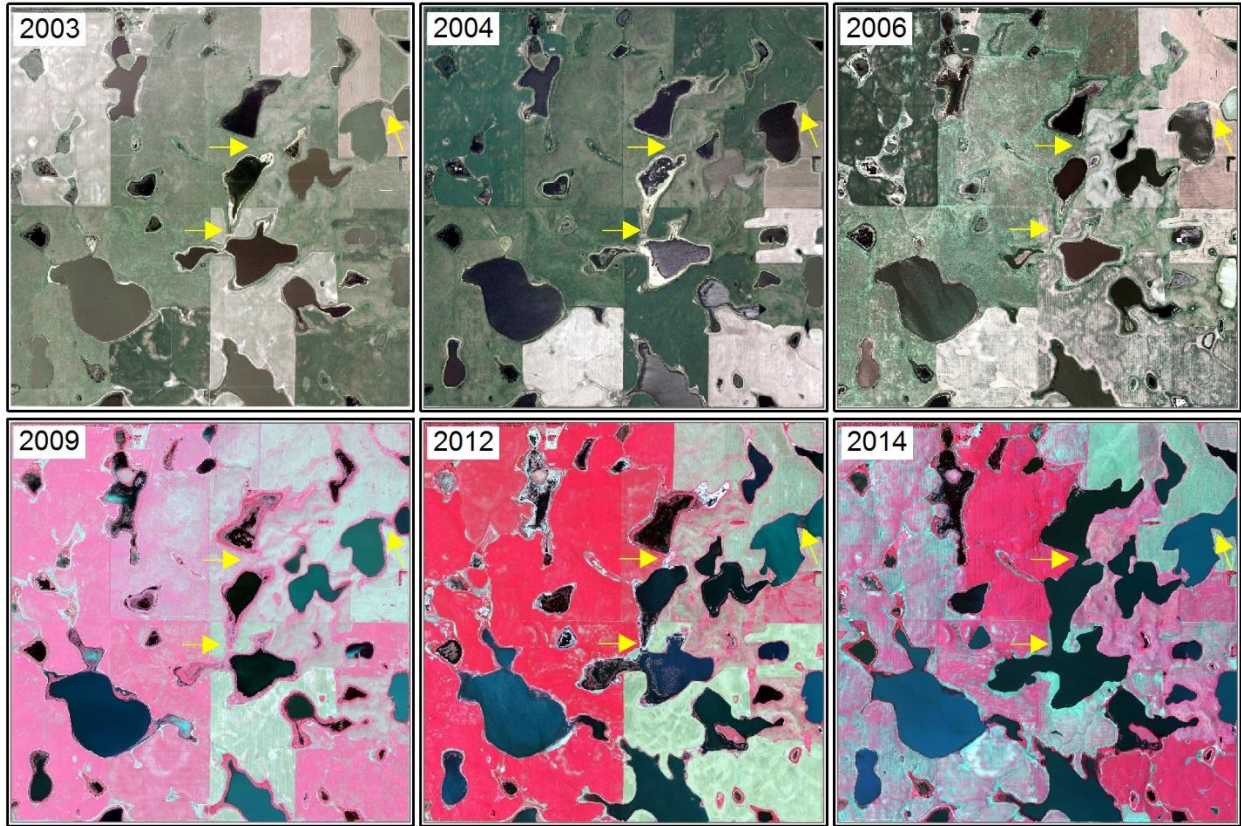
<b>Type</b>	<b>Count</b>	<b>Min (m)</b>	<b>Max (m)</b>	<b>Mean (m)</b>	<b>Median (m)</b>	<b>Sum (m)</b>
Ponding depth	<u>33,241</u>	<u>0.01</u>	<u>7.6</u>	<u>0.23</u>	<u>0.16</u>	<u>NA</u>
NHD flowlines	<u>1840</u>	<u>3.9</u>	<u><math>15.5 \times 10^3</math></u>	<u>762</u>	<u>317</u>	<u><math>1.4 \times 10^6</math></u>
Flow path length	<u>41,449</u>	<u>1.5</u>	<u><math>4.7 \times 10^3</math></u>	<u>138</u>	<u>83</u>	<u><math>5.0 \times 10^6</math></u>
Elevation difference	<u>41,449</u>	<u>0.01</u>	<u>70.9</u>	<u>2.1</u>	<u>0.89</u>	<u>NA</u>

693



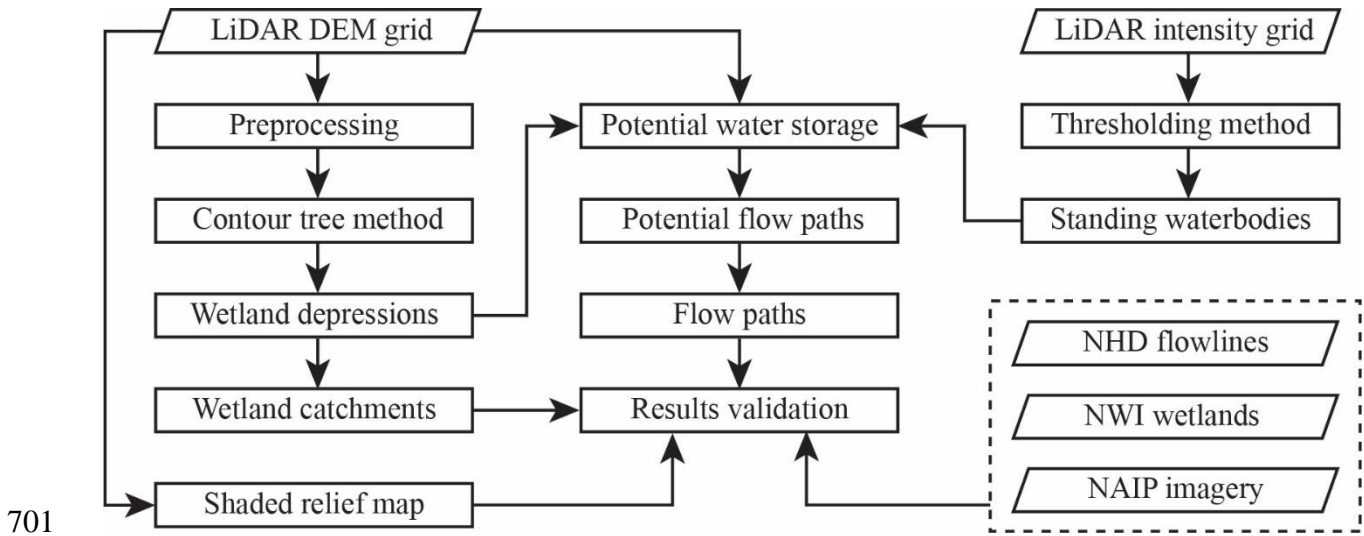
694

695 **Figure 1.** Location of the Pipestem subbasin within the Prairie Pothole Region of North Dakota.



696

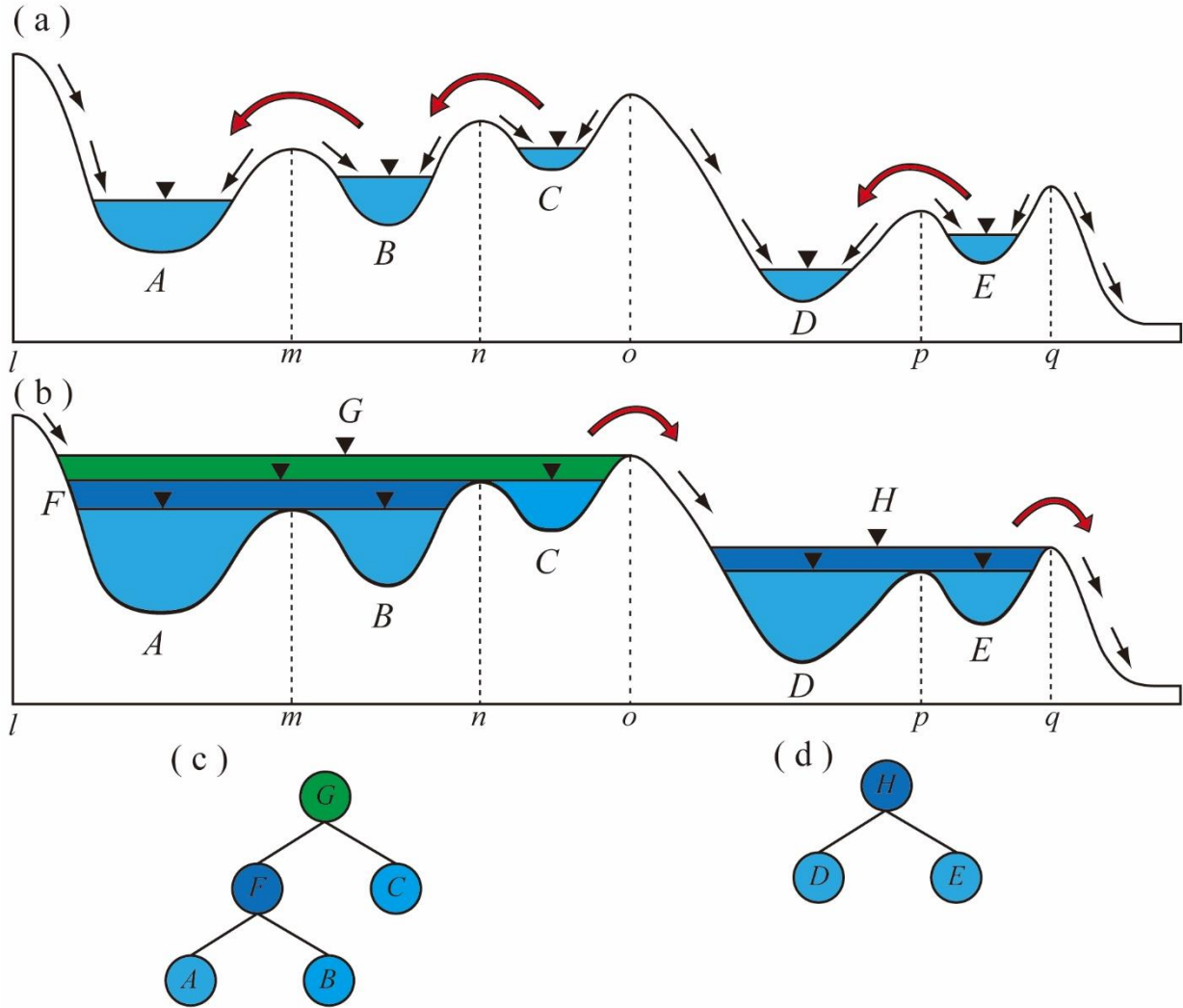
697 **Figure 2.** Examples of the National Agriculture Imagery Program (NAIP) aerial imagery in the Prairie Pothole  
 698 Region of North Dakota illustrate the dynamic nature of prairie pothole wetlands under various dry and wet  
 699 conditions. The yellow arrows highlight locations where filling-spilling-merging dynamics occurred (imagery  
 700 location: 99°8'34.454" W, 47°1'23.519" N).



701

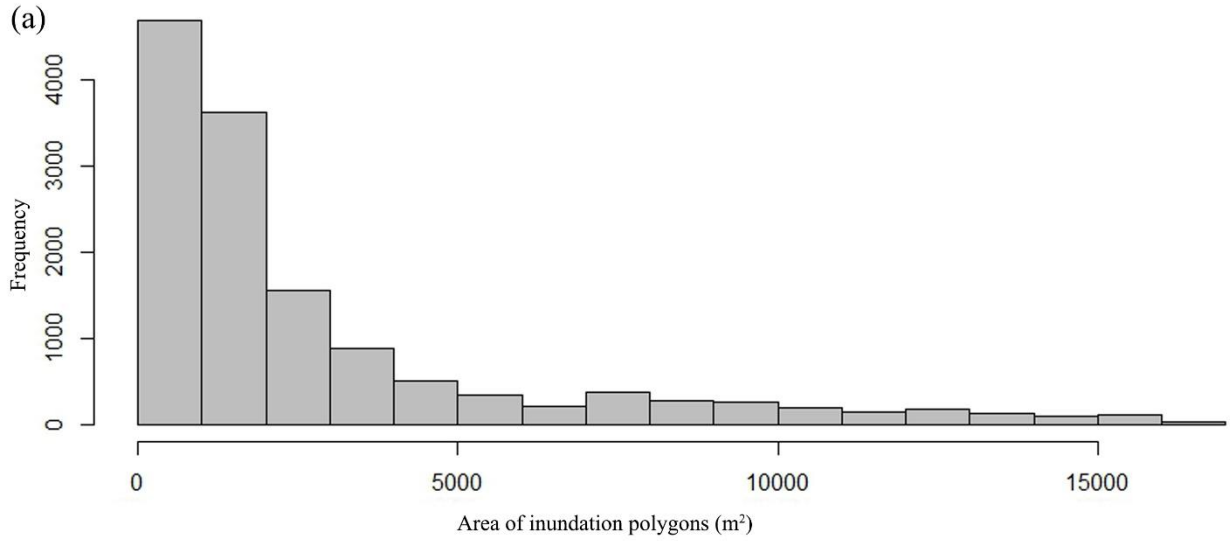
702

**Figure 3.** Flowchart of the methodology for delineating wetland catchments and flow paths.

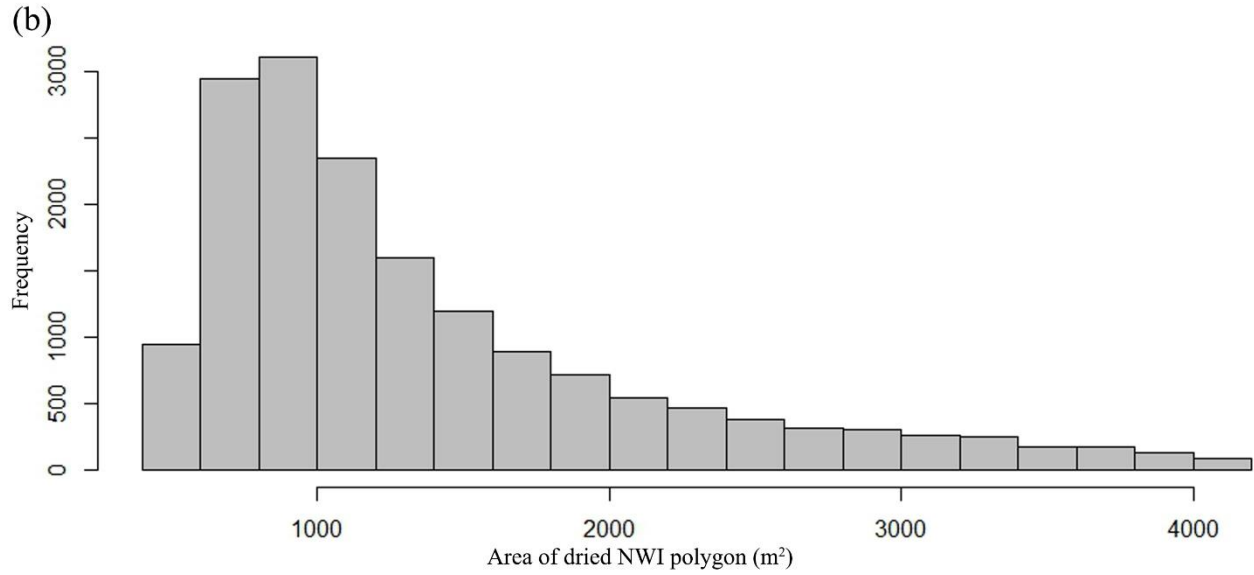


703

704 **Figure 4.** Illustration of the filling-merging-spilling dynamics of wetland depressions: (a) first-level depressions; (b)  
 705 nested hierarchical structure of depressions under fully-filled condition; (c) corresponding contour tree  
 706 representation of the composite wetland depression (left) in (a); and (d) corresponding contour tree representation of  
 707 the composite wetland depression (right) in (a). Different color of nodes in the tree represents different portions of  
 708 the composite depression in (a): light blue (first-level), dark blue (second-level), and green (third-level).



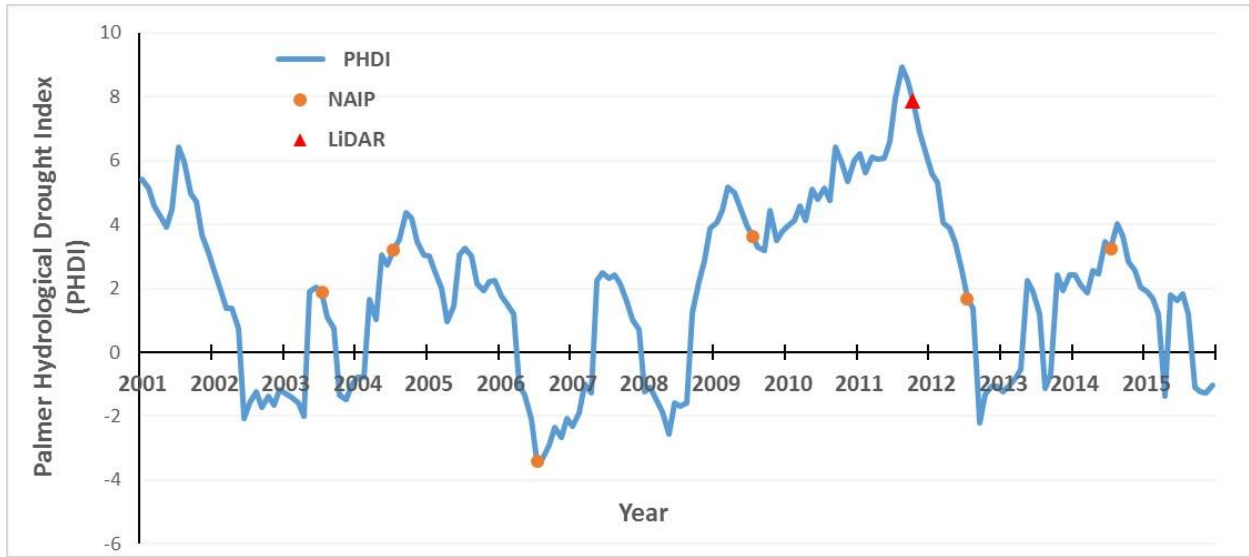
709



710

711 **Figure 5.** Histograms of inundation and NWI wetland polygons. (a) Inundation objects derived from LiDAR  
 712 intensity data; (b) dried NWI wetland polygons not intersecting inundation objects.



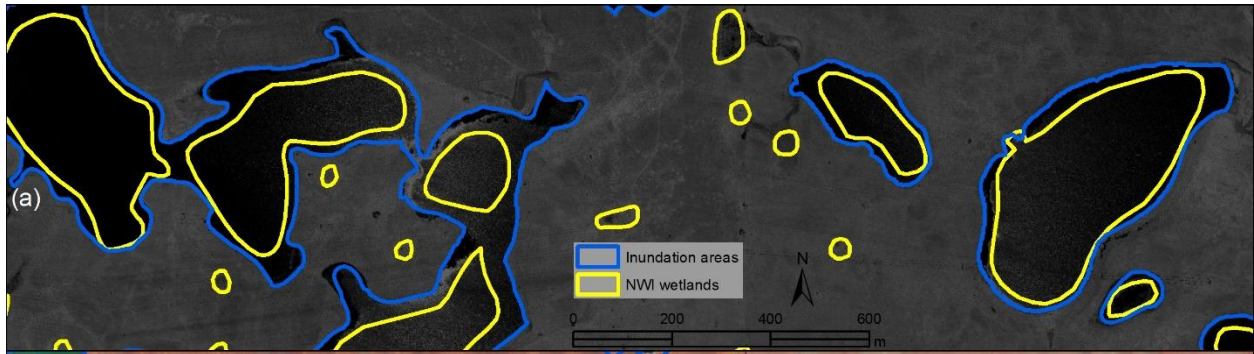


713

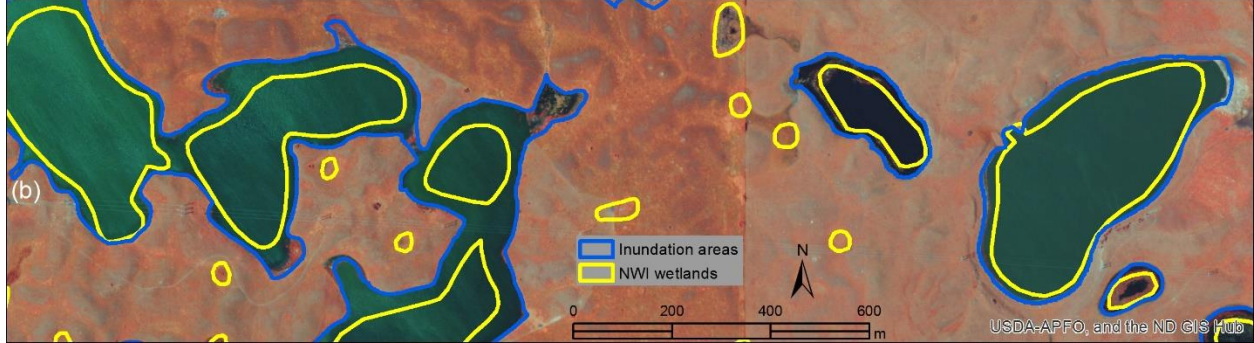
714

**Figure 6.** Palmer Hydrological Drought Index (PHDI) of the Pipestem subbasin (2001-2015).

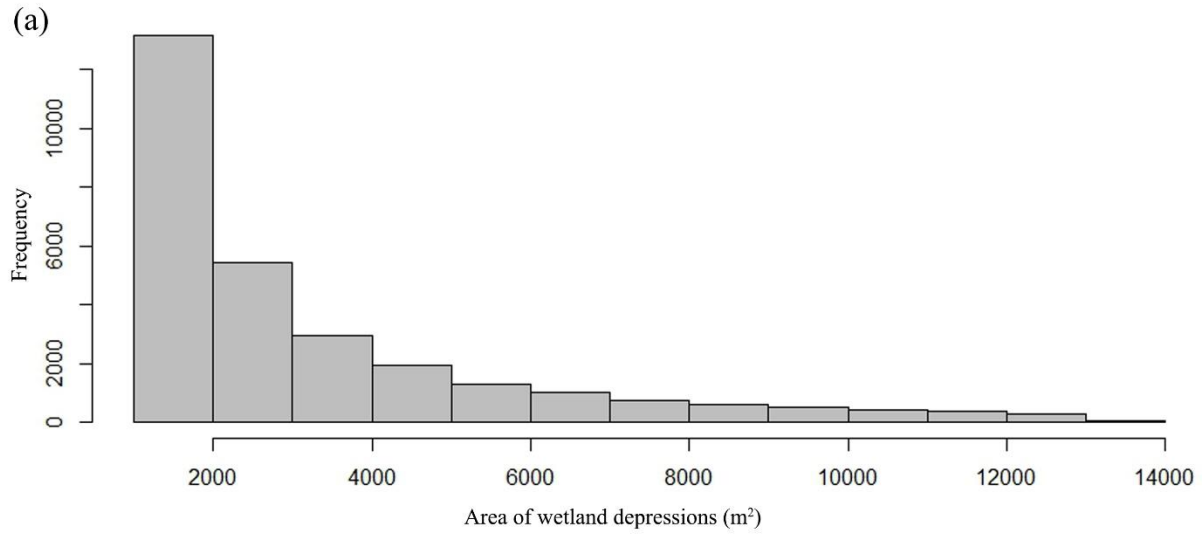
715



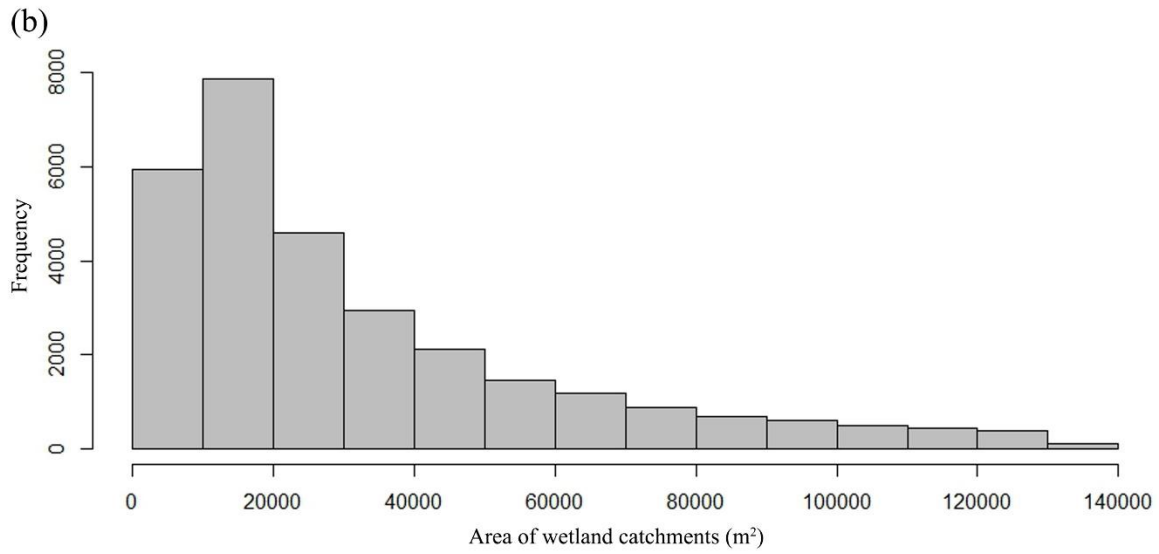
716



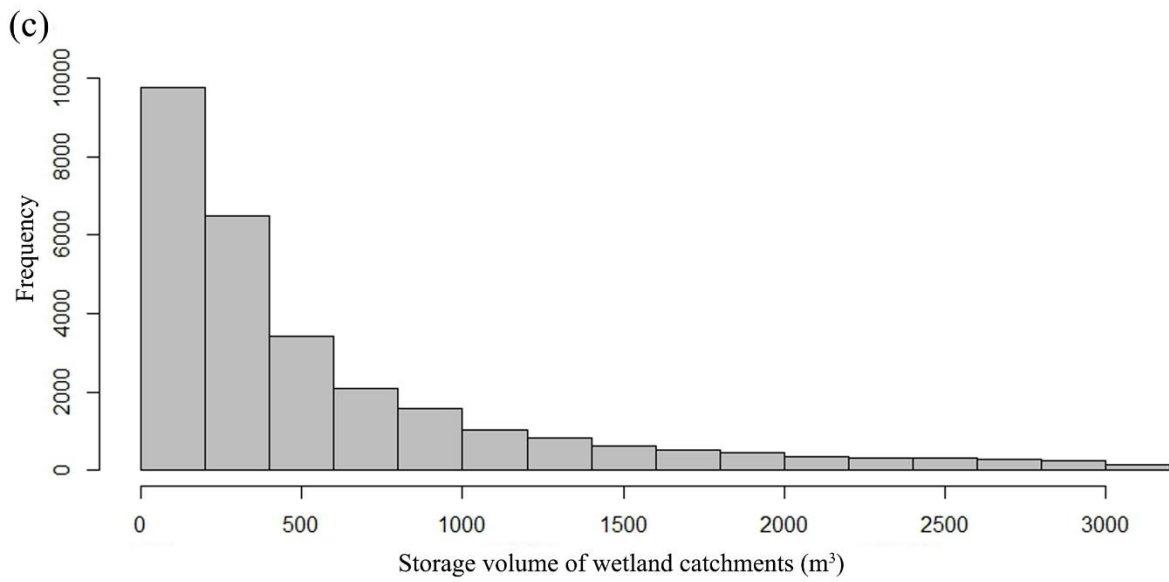
717 **Figure 7.** Comparison between inundation areas (derived from LiDAR intensity data) and NWI wetland polygons  
718 (image location: 99°9'53.9" W, 47°3'34.474" N). (a) Inundation areas and NWI wetlands overlaid on LiDAR  
719 intensity image; and (b) inundation areas and NWI wetlands overlaid on color infrared aerial photograph (2009).



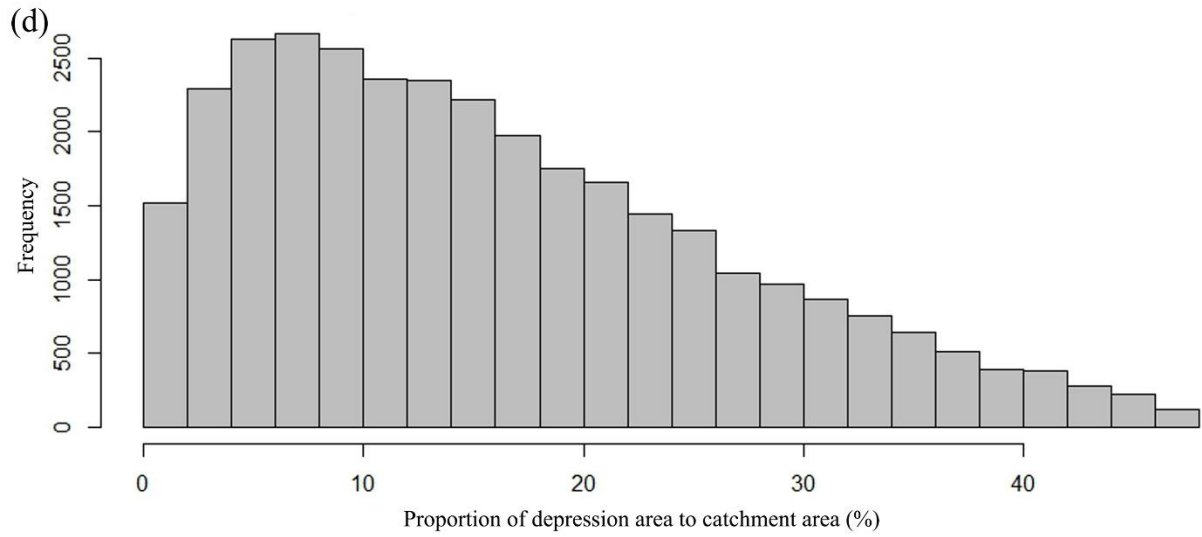
720



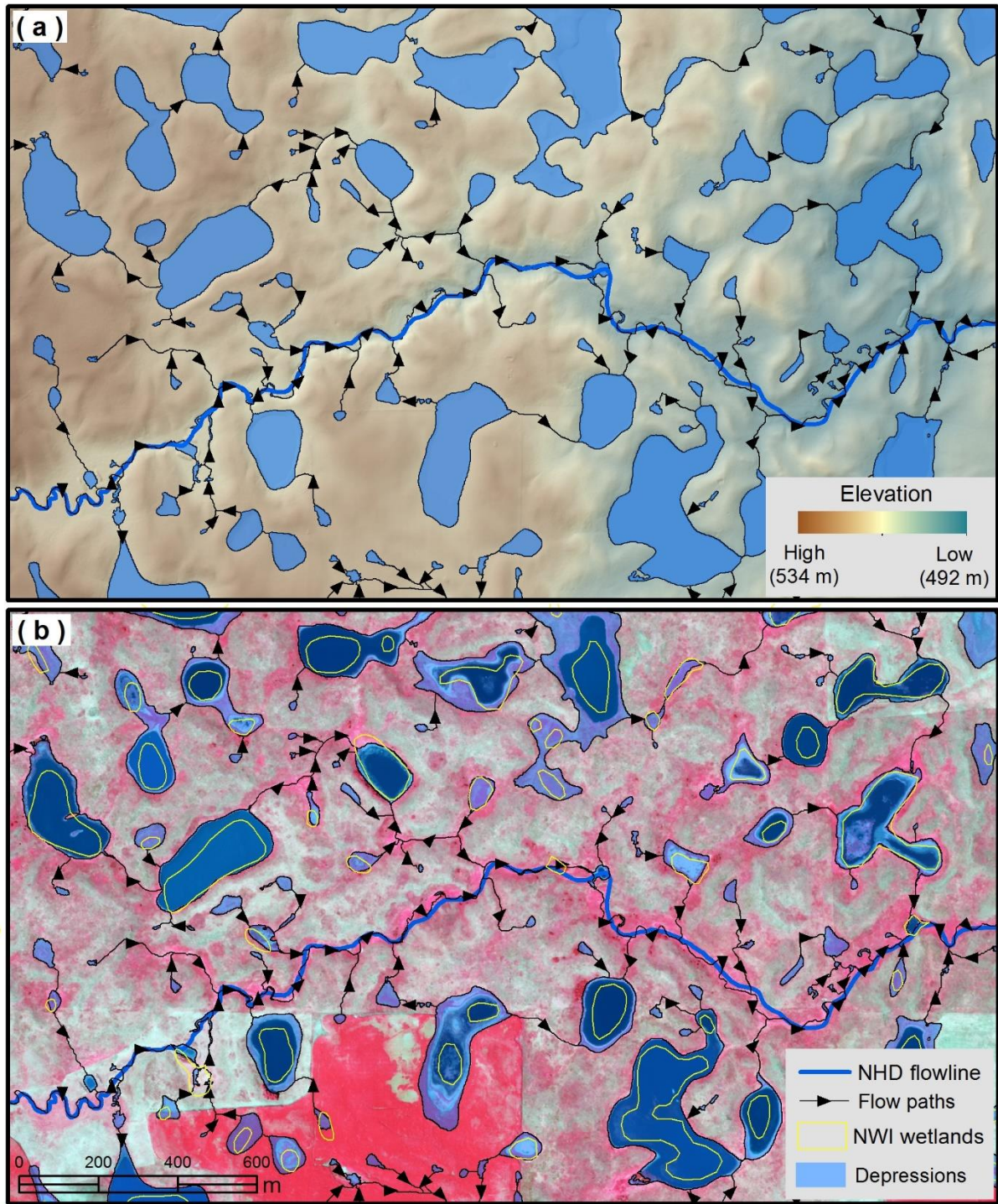
721



722

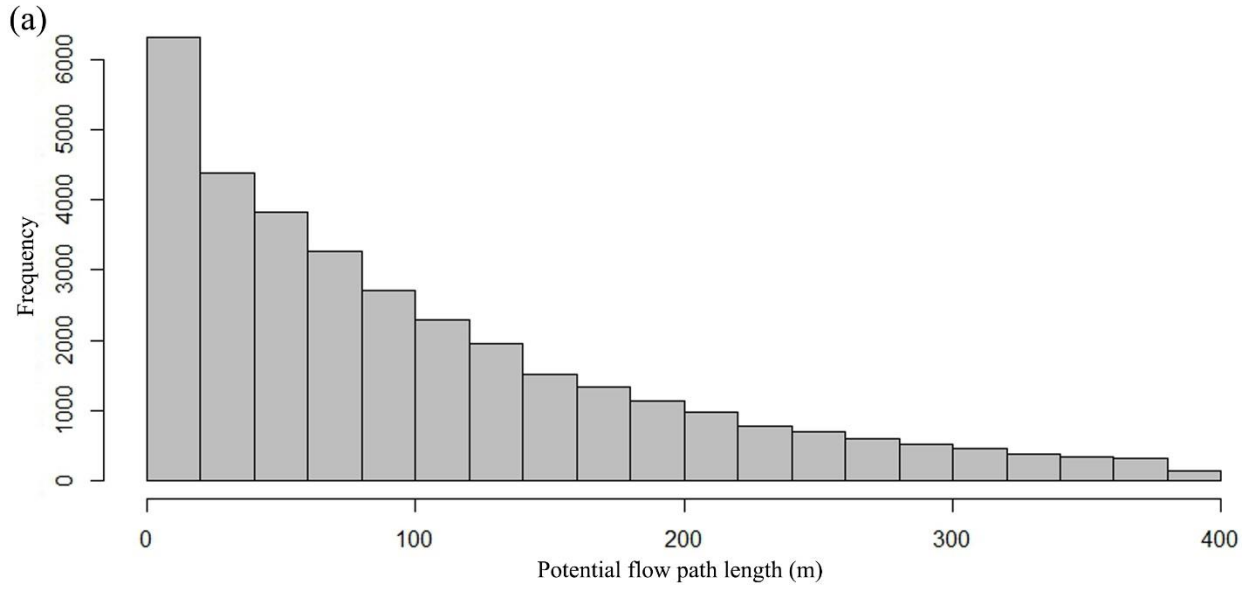


723  
 724 **Figure 8.** Histogram of wetland depressions and catchments. (a) Wetland depressions; (b) wetland catchments; (c)  
 725 potential storage capacity; and (d) proportion of depression area to catchment area.

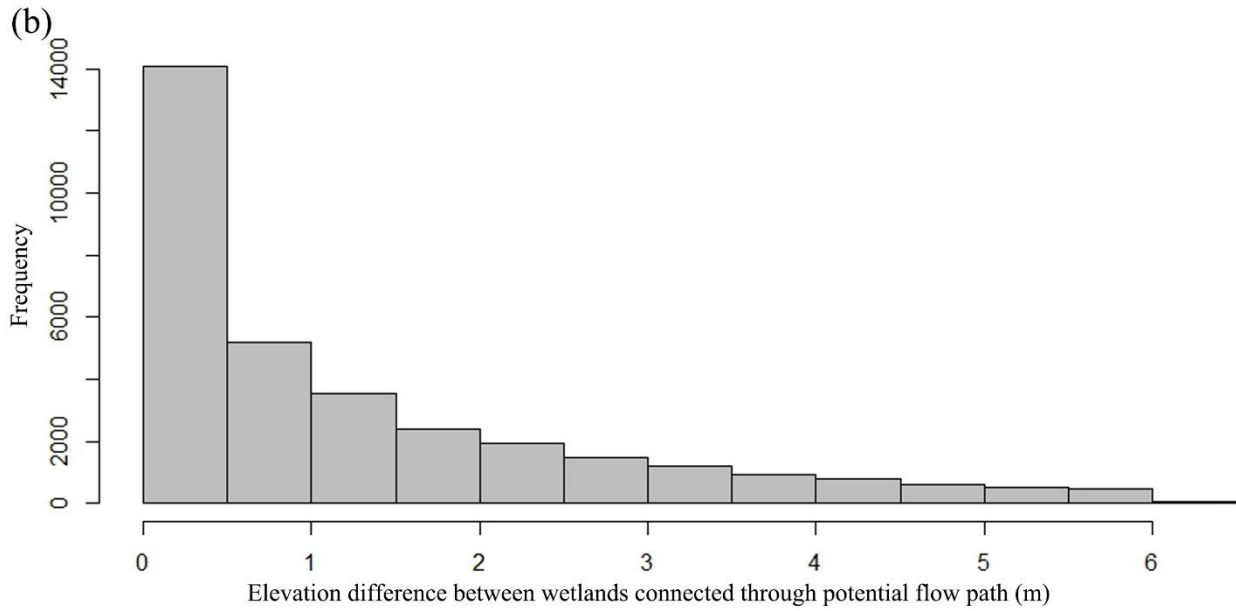


726

727 **Figure 9.** Examples of LiDAR-derived wetland depressions and flow paths in the Pipestem subbasin (image  
 728 location: 98°59'48.82" W, 47°1'32.679" N). (a) Wetland depressions and flow paths overlaid on LiDAR shaded  
 729 relief map; and (b) NWI polygons, wetland depressions and flow paths overlaid on color infrared aerial photograph  
 730 (2012).



731



732

733 **Figure 10.** Histogram of [potential](#) wetland connectivity. (a) [Potential Connectivity-flow path](#) lengths; and (b)  
 734 elevation differences between [connected](#)-wetlands [connected through potential flow paths](#).